



**Politecnico
di Torino**

Politecnico di Torino

Master's Degree in Computer Engineering

**Study and application of MIMO, LPV state observer
for industrial manipulators**

Supervisor

Prof. Marina Indri

Supervisor at Comau

Ing. Aldo Maria Bottero

Candidate

Matilde Zampolini

December 2024

Abstract

This thesis is carried out in collaboration with Comau S.p.A. The experimentation of state observers for the reconstruction of the angular velocity of the links of a flexible industrial manipulator has been performed, in the presence of unmodeled or uncertain parts. In a particular simplified condition in which there is only one axis moving at a time, a study was done to understand how faithfully the dynamics of the machine can be reconstructed using simple single axis models, extending them to take into account the multi-variable dynamics of the system and trying to reconstruct the action of non-linear friction as well. The observer model is braked into a nominal part that coincides with the dynamics of the center of mass of the robotic arm and a higher order part defined as “uncertainty function”, which changes the nature of the system from an isolated and single-variable system to a multi-variable system. This type of representation allows a significant reduction in model order, maintaining high accuracy in the reconstruction of the angular velocity of the center of mass. Various models of different complexities have been tested with both the asymptotic Luenberger observer and the steady-state Kalman filter. Furthermore, the difference in the reconstruction of the state is analyzed between a first approximation model and the identified model that better represents reality. The presence of friction is taken into account by a feedforward compensation or by the addition of a disturbance observer synthesized as a pole placement regulator.

First the observers are tested in simulation, then on real data from a Racer 7-1.0 robot, using both a normal trajectory and a more energized one. To evaluate the quality of the reconstruction, a virtual sensor obtained from the identification of the manipulator is used and then a final test is carried out with the real Xsens gyroscope.

Contents

| | | |
|----------|--|-----------|
| 1 | Introduction | 4 |
| 1.1 | Context | 4 |
| 1.2 | Objectives of the thesis | 5 |
| 1.3 | Structure of the thesis | 6 |
| 2 | State of the art | 7 |
| 2.1 | Flexible manipulators | 7 |
| 2.2 | Observers | 8 |
| 2.2.1 | Luenberger observer | 9 |
| 2.2.2 | Kalman filter | 10 |
| 2.2.3 | Extended state observer | 12 |
| 2.3 | Friction compensation | 13 |
| 2.3.1 | Model-based friction compensation | 13 |
| 2.3.2 | Disturbance observer | 13 |
| 3 | Problem analysis | 15 |
| 3.1 | Racer 7-1.10 | 15 |
| 3.1.1 | Robotic Toolbox | 16 |
| 3.1.2 | Moni toolbox | 16 |
| 3.1.3 | PDL language | 16 |
| 3.2 | Dynamics of a flexible manipulator | 17 |
| 3.2.1 | Inertia matrix | 18 |
| 3.3 | Linearization | 19 |
| 3.3.1 | Linear Parameter Varying (LPV) systems | 19 |
| 3.4 | Predictable torque | 20 |
| 3.5 | Discretization | 22 |
| 3.6 | Observer | 23 |
| 3.6.1 | 6-state observer | 24 |
| 3.6.2 | 5-state observer | 27 |
| 3.6.3 | 4-state observer | 28 |
| 3.6.4 | 7-state observer | 29 |
| 3.7 | Friction | 31 |
| 3.7.1 | Open chain simulation of friction | 31 |

| | | |
|----------|--|-----------|
| 3.7.2 | Synthesis of a pole placement regulator | 32 |
| 3.8 | Estimation of friction parameters | 35 |
| 3.9 | Model identification of the Racer 7-1.10 | 40 |
| 4 | Simulation results | 43 |
| 4.1 | Compensation of disturbances | 44 |
| 4.2 | 5-state Luenberger observer | 47 |
| 4.3 | 5-state Kalman filter | 49 |
| 4.4 | 6-state Luenberger observer | 50 |
| 4.5 | 6-state Kalman filter | 51 |
| 4.6 | 4-state Luenberger observer | 52 |
| 5 | Experimental results | 53 |
| 5.1 | Models comparison | 54 |
| 5.1.1 | Fit percentage | 54 |
| 5.1.2 | Nominal and identified data | 54 |
| 5.2 | Gravity and friction compensation | 55 |
| 5.3 | Motor torque disturbance compensation | 56 |
| 5.4 | Torque-current relationship | 57 |
| 5.5 | Virtual sensor | 58 |
| 5.5.1 | Final results with virtual sensor | 60 |
| 5.6 | Gyroscope | 60 |
| 5.6.1 | Trajectory at 400 Hz | 60 |
| 5.6.2 | Exciting trajectory | 64 |
| 5.6.3 | Final results with real gyroscope | 66 |
| 6 | Conclusions | 68 |

1. Introduction

The current thesis realized in collaboration with Comau S.p.A, an integrated society which develops and manufactures automation processes, production solutions and services, with a particular interest towards industrial manipulators and their application in automation processes (e.g., assembly, welding, and load lifting).

A precise position tracking is required during the process of performing tasks. Because of the high nonlinear flexibilities, time-varying and uncertain parameters, model error, frictional losses, and the influence of unknown noise in the model, the control of a robotic arm is always a complex operation. It requires link positions and velocities, and these quantities are not frequently measured on commercial systems.

In this perspective, the observer covers a fundamental role, since it is the basic element of multi-objective control architecture for simultaneous control of both manipulator position trajectory in the workspace and active damping of structural vibrations.

1.1 Context

The observer problem for flexible joint manipulator is one of the most important problems in robot control theory. The control of these robots by state feedback requires the knowledge of four state variables for each joint, which may be either positions and velocities of the motors and the links, or positions, velocities, accelerations and jerks of the links.

Unfortunately, in many real-world situations not all the state variables of a system are measured and even though a variable is measured, it may be subject to relevant disturbances or errors.

Motor positions can be easily extracted from encoders placed on the manipulator, as well as motor velocities by taking the first derivative of previous measurements, but sensors that directly measure link position and velocity are rarely used.

Although sensors improve the overall precision of the manipulator's movement, they can also degrade a control system as they present four main problems: [1]

1. Economical cost: they represent the most expensive components of the control architecture.
2. There are not many sensors that are capable of resisting machine wear over time.
3. Diagnostics management: it is difficult to detect if they are breaking.
4. Mathematical control problems: all the sensors that are far from the actuators always produce a signal that has two parts, a useful part that can be easily used and a part that is deterministic

noise. The sensors must then be filtered through an observer and this adds complexity.

Observers are virtual sensors that estimate the state of a system from input/output measurements. They can be useful to:

- Estimate variables that are not measured (thus saving money and space)
- Increase safety and fault tolerance
- Improve the accuracy of sensors via a suitable data fusion, attenuating the disturbance/error effects.

The observer allows also to correct the errors introduced by the uncertainties on the model. The models used are approximations of a reality that is very complex, of a much higher order.

1.2 Objectives of the thesis

The objective of the thesis is the experimentation of state observers for the reconstruction of the angular velocity of the links of a Racer 7-1.0 industrial non-rigid manipulator, in the presence of unmodeled or uncertain parts.

The minimum application requirements are:

- Ability to distinguish between the driving torque that changes the state of the system and friction.
- Manage the interaction between simple decoupled systems: understand how to increase the state of the system to represent and reconstruct the non-modeled parts of the system; understand how to place the poles to be able to have the maximum possible advantage in reconstructing the state and the minimum possible impact from measurement disturbances.
- Minimum characterization (identification) of the Racer 7-1.0 manipulator to have a realistic model of the two considered axes (2 and 3).
- Analysis of the difference between the use of first approximation nominal models and the use of identified machine models to highlight the fact that observers work well if the model is well aligned with reality.

There exist two possible solutions:

1. Multi-variable (MIMO) observers: good results have already been obtained, but they are very complex objects. Managing the recalculation of all terms in real time is heavy. This solution is not taken into account in this thesis.
2. Single-variable (SISO) observers, one for each axis (only axis 2 is considered in this case): it is a more industrial approach. The axis is not isolated, but an interacting model is adopted that must satisfy some characteristics:
 - Have some additional state that helps to reconstruct the interaction: it is as if a simplified model of the interactions is included in the state, that otherwise would not have been taken into account in the nominal model of the joint.

- Have an external observer for each axis (disturbance observer) which reconstructs the friction components that are not immediately estimated and the effect of other motor input disturbances not modeled at low frequency.

First the observers are tested in simulation, then on real data from the machine. To evaluate the quality of the reconstruction, a virtual sensor obtained from the identification of the manipulator is used and then a final test is carried out with the real gyroscope.

The aim of the work is to highlight the advantages and disadvantages of the various solutions (which one performs better, which costs more in terms of implementation, complexity) and understand what is the minimum structure of the observer capable of best reconstructing the state.

1.3 Structure of the thesis

In Chapter 2, a review of the current state of the art is provided: concepts on flexible manipulators, on the asymptotic Luenberger observer, on the Kalman filter, and on friction compensation methods are recalled.

Chapter 3 makes an analysis of the specific problem: the manipulator used for the thesis is described, the dynamics of flexible manipulators, the various models of observers tested, the friction management methods, the method of estimating the friction parameters and the identified model of the manipulator.

Chapter 4 presents the experiments conducted in simulation, along with the obtained results.

In Chapter 5 the results of the tests on real data coming from the machine are presented, both using a virtual sensor and the real gyroscope.

The final chapter, Chapter 6, discusses the achieved results and suggests potential future works to continue this study.

2. State of the art

The problem of modeling an observer who is capable of obtaining an estimate of the state of a flexible industrial manipulator in the presence of uncertain parts has been much studied in literature. This chapter describes flexible manipulators, the properties of the asymptotic Luenberger observer, the Kalman filter and the Extended state observer. In conclusion, the friction compensation methods are presented.

2.1 Flexible manipulators

The standard assumption that is made for the design of robot kinematics, dynamics and control is that manipulators consist only of rigid bodies. This is, however, an ideal situation that can only be considered valid for slow movements and small interacting forces [2] (it is a limit in situations where the vibration effects are consistent). In a real case, the elasticity of the joints must be considered. Considering elastic phenomena is important when high speeds or higher levels of accuracy must be achieved.

In recent years, flexible joint manipulators (FJMs) are playing an increasingly important role in industrial production, medical, aerospace and other fields. Their advantages with respect to rigid robotic manipulators are: lightweight, smaller dimensions, higher operational speed, lower cost and lower power consumptions. However, problems like resonance phenomena and high nonlinearities are introduced by the drive system's elasticity [3]. Moreover, the FJMs in practical applications may inevitably suffer from various kinds of uncertainties including parameter perturbations, unmodeled dynamics and external disturbances.

It is possible to identify sources of oscillation (vibration in the manipulator) mainly in:

- Elasticity of the transmission (gearboxes, drive belts, long shafts): they generally cause the lowest resonant frequency of the system. Gear teeth are like flexible shafts, the movement between the teeth gives rise to elastic deformation.
- Distributed elastic deformations: “link stiffness” is always an ideal assumption and may fail when increasing payload/weight ratio, movement speed, control bandwidth.
- Presence of parasitic degrees of freedom: they are non-ideal constraint reactions and they introduce parasitic elastic joints with parasitic resonance effects.

The following hypotheses are formulated:

1. The joint deflection is small, so flexibility effects are considered within the linear elastic domain.

2. The deflection of the link in the plane of rotation of the joint and the elasticity of the gear are represented as an elastic joint connecting the actuator output shaft to a rigid link.
3. Motor rotors are assumed to have their center of mass on the axis of rotation. Therefore, the inertia matrix and the gravity vector are independent of the angular position of the motor.

Under certain conditions, the first resonant frequency is correctly predicted by the well-known model of two masses connected via an elastic element, represented in Figure 2.1. The motor, gearbox and load assembly is assumed to be an elastic coupling between two rigid bodies.

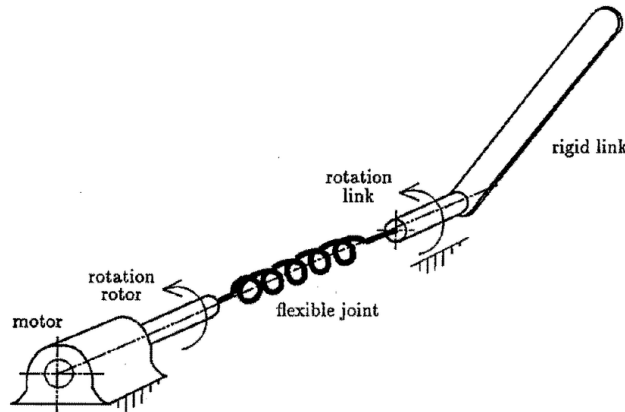


Figure 2.1. Model of two masses connected via an elastic element [4]

2.2 Observers

An observer is a dynamical system which, using as its inputs the output $y(t)$ and the input $u(t)$ of a dynamical system, generates as output an estimate $\hat{x}(t)$ of the state $x(t)$. In Figure 2.2 there is a schematic representation of the system.

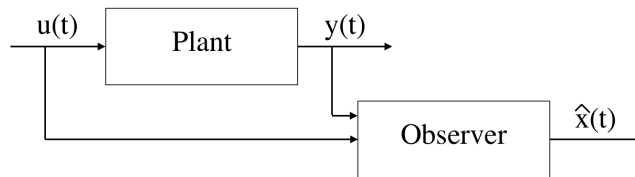


Figure 2.2. Observer

For a state estimator, we define the estimate error as the difference between the estimated state and the true state:

$$e(t) = \hat{x}(t) - x(t) \quad (2.1)$$

An estimator for which the estimate error goes to zero as time approaches infinity is called an asymptotic state observer.

$$\lim_{t \rightarrow \infty} \|e(t)\| = \lim_{t \rightarrow \infty} \|\hat{x}(t) - x(t)\| = 0 \quad (2.2)$$

The use of an asymptotic state observer guarantees that estimates with asymptotically zero error are obtained.

2.2.1 Luenberger observer

A Luenberger observer is an asymptotic state estimator for linear systems.

For discrete-time Linear Time Invariant (LTI) systems the asymptotic estimator takes the form:

$$\begin{cases} \hat{x}(k+1) = A\hat{x}(k) + Bu(k) - L(\hat{y}(k) - y(k)) \\ \hat{y}(k) = C\hat{x}(k) + Du(k) \end{cases} \quad (2.3)$$

In Figure 2.3 there is a schematic representation of the Luenberger observer.

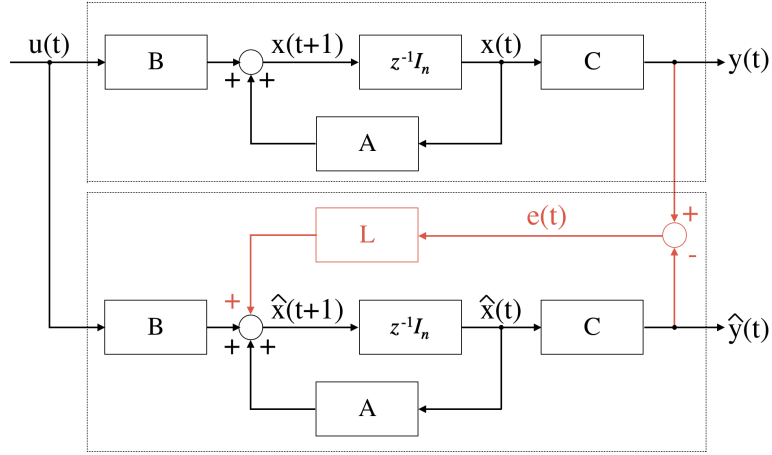


Figure 2.3. Block diagram representation of the Luenberger observer

To take into account the measurement of the output y in the equations, the correction term $-L(\hat{y}(k) - y(k))$ is added. Therefore the condition $\lim_{t \rightarrow \infty} \|e(t)\| = 0$ will be satisfied only if $(A - LC)$ has asymptotically stable eigenvalues.

The following theorem holds: If the dynamic system

$$\begin{cases} x(k+1) = Ax(k) + Bu(k) \\ y(k) = Cx(k) + Du(k) \end{cases} \quad (2.4)$$

where $x(t) \in \mathbb{R}^n$, $u(t) \in \mathbb{R}^p$, $y(t) \in \mathbb{R}^q$, is completely observable, then it is always possible to find a matrix L allowing to arbitrarily assign all the eigenvalues of the matrix $(A - LC)$. If the system is not fully observable, dynamics cannot be arbitrarily imposed to the estimate error, since only the eigenvalues of the observable part can be modified.

Theory says that the system (2.4) is fully observable if the observability matrix:

$$M_O = \begin{bmatrix} C \\ CA \\ \vdots \\ CA^{n-1} \end{bmatrix} \quad (2.5)$$

is full rank, i.e., $\rho(M_O) = n$.

In MatLab, the gain matrix L can be computed, in the case of eigenvalues of unitary multiplicity, using the `place` command: `L = place(A',C',p)'`, where A , C are the state matrices, p is the vector containing the eigenvalues to assign.

The selection of the observer poles is a compromise between sensitivity to measurement errors and rapid recovery of initial errors. A fast observer will converge quickly, but it will also be sensitive to measurement errors.

2.2.2 Kalman filter

In the case of the Luenberger observer the rapidity with which the estimate error goes to zero is established through the frequencies imposed to the eigenvalues. Increasing the frequency of the poles, the speed of convergence of the error increases, but also the noise. However, to make a Luenberger observer, systems must be fully observable and that is a very strong request.

On the other hand, the Kalman filter has quadratic stability based on a Lyapunov function. The observer asymptotically gives an estimate of the state, but the speed of convergence to zero of the estimate error cannot be established. However, it can also be used with systems that are not fully observable.

The Kalman filter is a recursive filter that evaluates the state of a dynamic system starting from noisy measurements.

Systems subject to uncorrelated process noise $v_1(k)$ and measurement noise $v_2(k)$ are considered. The state space equations of a discrete-time Linear Time Invariant (LTI) system with noise are:

$$\begin{cases} x(k+1) = Ax(k) + Bu(k) + v_1(k) \\ y(k) = Cx(k) + v_2(k) \end{cases} \quad (2.6)$$

The noises are assumed to be uncorrelated, white and Gaussian.

The Kalman filter works by propagating the estimate of the mean and covariance of the state over time. Like many other state-of-the art observers, it is based on the following operations:

1. Prediction: at time $k - 1$, compute a prediction $\bar{x}(k)$ of the state $x(k)$ and a prediction \bar{P} of the covariance P of the estimation error, using the system model:

$$\bar{x}(k) = A\hat{x}(k-1) + Bu(k-1) \quad (2.7)$$

$$\bar{P} = APA^T + Q \quad (2.8)$$

2. Update: at time k , the prediction $\bar{x}(k)$ is corrected using the output measurement $y(k)$, giving the

"more accurate" estimate

$$S = C\bar{P}C^T + R \quad (2.9)$$

$$K = \bar{P}C^T S^{-1} \quad (2.10)$$

$$\hat{x}(k) = \bar{x}(k) + K(y(k) - C\bar{x}(k)) \quad (2.11)$$

$$P = (I - KC)\bar{P} \quad (2.12)$$

where K is the gain matrix, chosen to minimize the variance of the estimation error norm

$$\|x(k) - \hat{x}(k)\|_2^2 \quad (2.13)$$

Q is the covariance matrix of $v_1(k)$, R is the covariance matrix of $v_2(k)$.

Through simple operations, we obtain:

$$\bar{P} = A(\bar{P} - \bar{P}C^T(C\bar{P}C^T + R)^{-1}C\bar{P})A^T + Q \quad (2.14)$$

$$K = \bar{P}C^T(C\bar{P}C^T + R)^{-1} \quad (2.15)$$

The first of these equations is called discrete algebraic Riccati equation. The second one gives the filter gain matrix.

Putting all the equations together, the general form of the Kalman filter is the same as that of the Luenberger observer:

$$\begin{cases} \hat{x}(k+1) = A\hat{x}(k) + Bu(k) - K(\hat{y}(k) - y(k)) \\ \hat{y}(k) = C\hat{x}(k) + Du(k) \end{cases} \quad (2.16)$$

The gain matrix K is proportional to the uncertainty in the state estimate and inversely proportional to that in the measurements. If the state estimate is relatively precise, the Kalman gain has not a high impact on updating the state estimate, and consequently the Kalman filter trusts the system model more; otherwise, if the state estimate is quite uncertain, the Kalman gain is high and, consequently, the Kalman filter trusts the sensor measurements more than the system model.

In Matlab, the gain matrix K can be computed using the `kalman` command, which calculates the gains given the state-space model of the system and the covariances of the process and measurement noise.

An extended Kalman filter (EKF) is developed in [5] for precise estimation of the position of the end-effector of a two-axis robotic arm with flexible links by employing direct end-effector position measurements in addition to the standard joint position measurements. Two states are added to the EKF's model in order to partially compensate for the joint angle encoder calibration errors and kinematic errors. The dynamics of these states was represented by a zero-derivative since they reflect bias errors in the joint angle measurements.

Covariance matrices design

The Kalman filter design is based on the choice of the covariance matrices Q and R . The performance of the Kalman filter is highly affected by Q and R . These matrices can be defined from the available information on $v_1(k)$ and $v_2(k)$.

- R is the diagonal covariance matrix of the measurement noise of the type $R = eye(n) \cdot \sigma^2$, where σ^2 is a vector containing the standard deviation of the measured values from the real values obtained from measurements on a real machine.
- Q is a positive symmetric covariance matrix of the type $Q = G \cdot G^T$, which represents all process noises affecting the system (e.g. unmodeled dynamics and parameter uncertainties). The values on the diagonal are directly related to the corresponding states. Off-diagonal values represent interactions between different states. This matrix is usually obtained with trial-and-error techniques, which rely on users' experiences and background.

In general, a high value of Q means a big system noise, and it also indicates the increase of model uncertainty. On the other hand, a big value of R indicates the strong measuring noise. Simulation results indicate that the ratio module of Q and R could decide the system instantaneous response.

In [6], an estimation approach is proposed to adaptively adjust Q and R matrices at each step of the Extended Kalman filter (EKF) to improve dynamic state estimation accuracy. Different from the state-of-art Kalman filter, which keeps the covariance matrices constant, they are updated during each correction step. An innovation-based method is used to adaptively adjust Q . A residual-based method is used to adaptively adjust R . However, users need to select adequate initial values for Q_0 and R_0 in the initialization step.

2.2.3 Extended state observer

The Kalman filter works to reconstruct the state variables and takes into account (in the form of a random process with a certain covariance) the presence of non-measurable exogenous signals, but does not reconstruct them. If we want to reconstruct them, both in the Kalman filter and in the asymptotic Luenberger observer, an additional state must be added.

Because of its simple structure and high efficiency, extended state observer (ESO) is used extensively in robotics, aerospace, and electrical mechanics.

In [7], a linear extended state observer (LESO) is designed to implement a feedback linearization-based control law, proposed for the trajectory tracking control of a single-link flexible-joint robotic system. The control law requires knowledge of all the states, therefore the goal of the ESO is to estimate the state vector, as well as the uncertainties. In contrast to conventional observers, the ESO estimates the effect of uncertainties, unmodeled dynamics, and external disturbances acting on the system as an extended state of the original system. Assuming a small rate of change of uncertainty, the ESO error dynamics show asymptotic stability. Otherwise, if the r -th rate of change of uncertainty is negligible, an r -th order ESO can be designed.

In [8], it is shown that, when compared to the first-order ESO, the higher order ESO can provide better state estimation for sinusoidal disturbances as long as the observer bandwidth is chosen to be substantially larger than the disturbance's frequency and sufficiently smaller than unmodeled high frequency dynamics.

In [9], an improved version of the ESO is designed to separate the estimation of the total disturbance from the reconstruction of system states. A new parameter is employed to adjust disturbance estimation instead of the bandwidth of the observer.

In most practical cases, system output is corrupted by measurement noise. Influence of the noise on system performance is greater, if observer bandwidth is wider. In order to reduce the influence of noise, in [10] a first order low-pass filter is designed and added into the design of ESO. This procedure

separates most of the noise from the input signal, and the observer's estimation ability is improved. However, the low-pass filter also introduces a time-delay. The time-delay and the system time response may be a trade-off in real time control.

In [11], the extended state observer is used to estimate both the unmeasurable system states and acting lumped disturbance. In order to obtain fast convergence in ESO, high gains are typically required, which may make it sensitive to measurement noise. A structure composed by a Kalman filter and ESO is proposed in order to get over this restriction. While the latter is in charge of online state and disturbance reconstruction, the former acts as noise filtering.

In [12], a state observer for a two-link flexible arm has been analyzed. It receives as measured quantities joint position and velocity and three deflection measurements obtained through an optical transducer. The presence of vibration modes and noisy deflections requires the observer to perform a filtering action, achieved with a Kalman-Bucy filter, which finds the best linear estimate of the state by calculating the steady state filter gain matrix.

2.3 Friction compensation

The problem of estimating and suppressing disturbances has wider applications than just countering the influence of the external environment: disturbances can also be understood as uncertainty in the plant's parameters, discrepancy between the adopted model of the plant dynamics and its behavior, nonlinearities present in the system, and the influence of other factors. Suppression of such disturbances makes it possible to improve the robustness of the control system in relation to these conditions.

Friction is a natural physical phenomenon that governs the functioning of all machines. For robots with flexible joints the effects of joint friction can strongly influence the system performance, especially for robots with high gear ratio and for high-speed applications. For these reasons, friction modelling, identification, and compensation have been addressed by a number of researchers.

2.3.1 Model-based friction compensation

A simple method is model-based friction compensation that requires to know a precise friction model. However, friction is a highly nonlinear, complex phenomenon and its parameters can vary with time, joint position, load or with temperature. So, model based friction compensation is quite inaccurate.

2.3.2 Disturbance observer

One of the most promising methods is observer-based control where a Disturbance Observer (DO) or a Proportional-Integral Observer (PIO) is used to estimate friction and unknown inputs affecting the system. This method has the advantage of being model-free and has been shown to be effective in practice to reject frictional effects. In case of flexible joint robots with joint torque measurements after the gearbox, one can distinguish between external loads acting on the link side of the robot and the internal friction disturbance acting mostly on the actuator.

In [13], a linear disturbance observer for friction compensation was proposed for flexible joint robots with joint torque sensing in order to increase the positioning accuracy and the performance of torque control. For the analysis, a standard friction model containing Coulomb friction and viscous friction is considered. The result is that the design of the friction observer can be done independently of the MIMO

controller design, whereas when adding an integrator all gains of the controllers have to be changed for good performance.

A Nonlinear Disturbance Observer (NDO) for two-link robotic manipulators is presented in [14]. A revised friction model is used, due to the discontinuity of the friction characteristics at zero velocity. By carefully selecting the observer gain function, global convergence is guaranteed, based on Lyapunov theory. The disturbance is assumed to vary slowly relative to the observer dynamics.

In [15], a systematic design procedure is derived for a disturbance observer for the compensation of low-frequency disturbances. The principle of separation, which applies for an asymptotic state observer, also holds for the disturbance observer. Therefore, the poles of the closed-loop system can be placed independently from the poles of the augmented observer.

3. Problem analysis

This chapter describes the manipulator used for the experimentation, the dynamics of flexible manipulators, the method used for gravity compensation, the various observer models tested, the management methods of friction, the procedure for obtaining an estimate of the friction parameters and, in conclusion, the identified model of axis 2 of the considered manipulator is shown.

3.1 Racer 7-1.10

The Racer 7-1.10 robot, built by COMAU S.p.A., is a robot intended for typically industrial purposes.



Figure 3.1. Racer7-1.10

The external controller contains a PLC, the electric drives, the industrial CPU, the hardware and software necessary for programming and moving the robot, the Teach Pendant (i.e., the interface with the user), and the control algorithm of the robot. The simplest way to exchange information with the machine is via the USB port (there is also the possibility of connecting to the Ethernet network).

It is an anthropomorphic robot with 6 degrees of freedom (6 DOFs). The six joints, all revolute, can be divided into two groups: the first three represent the arm, the second three the wrist. The robot has a flange on which loads are attached to be manipulated or tools to perform operations.

Since the entire 6 DOF industrial manipulator is complex, an approximation of the 2-link non-rigid industrial manipulator is considered (only axes 2 and 3 are considered, while the other links are kept fixed, like a SCARA vertical robot).

3.1.1 Robotic Toolbox

`RobotTlbx5.0` is the robotics toolbox. It was derived by Peter Corke, who created tools that are valid for introducing the study of robotics. COMAU has included the specific characteristics of its industrial products.

The `get_robot` function creates the robot object and its copy, `RobotObject`, which can be used as a “universal parameter” by some standard applications. Each robot object is connected to an INIT file that contains all the robot’s data.

3.1.2 Moni toolbox

`Moni` is a toolbox that concerns the management of the binary files that we take from the control.

We are able to acquire from the control the position measurements of the encoders (the target and the real position of the motor) and the currents that the controller produces and sends to the drives.

`moni.log` are binary files that contain a set of onboard signals that are recorded synchronously every 2 ms.

The units of measurement used in COMAU models are:

- Current in Ampère/peak (A_p)
- Motor position in radiants
- Joint positions in degrees (they have right-handed and left-handed conventions)

The entire simulation environment uses the Denavit Hartenberg (DH) conventions, measuring the current in Ampère and the positions in radians with right-handed conventions (international system’s conventions).

3.1.3 PDL language

The machine movement programs are written in PDL language, that is similar to Pascal, with appropriate modifications.

It is a concurrent programming language. Parallel processes that perform different operations can be generated and synchronization constraints are created among them. The ability to have a workspace of common variables is typical of industrial automation languages, because it allows information to be exchanged dynamically.

The fundamental instruction to move the machine is `MOVE`, whose syntax is:

`MOVE <trajectory> <destination> <options>`

Since it is only possible to perform "point-to-point" type movements, for each `MOVE` it is always necessary to specify the arrival point and the type of trajectory to follow to reach that point.

3.2 Dynamics of a flexible manipulator

The dynamics of the non-rigid manipulator can be approximated with a lumped parameter model, in which arms are considered as rigid bodies and concentrated stiffness parameters are associated, in the form of torsional (and/or linear) springs in revolute (and/or prismatic) joints.

The model may contain non-powered degrees of freedom to approximate torsions and bendings directions that are not implemented by electric motors. These additional axes, sometimes called parasitic axes, represent non-ideal and non-rigid constraint reactions.

Considering a model with only elastic joints actuated (by motors), we obtain the Spong's model [16] (first introduced in 1985-1987), that is the first model in which robots began to be considered as non-rigid systems. The model is nonlinear and is divided into three groups of equations:

$$M(q)\ddot{q} + C(q, \dot{q})\dot{q} + G(q) + f_l(\dot{q}) + \beta_l\dot{q} = \tau_l \quad (3.1)$$

$$J_m\ddot{q}_m + \beta_m\dot{q}_m + f_m(\dot{q}_m) + Ntr^{-1}\tau_l = K_t I_{ref} \quad (3.2)$$

$$\tau_l = K(Ntr^{-1}q_m - q) + \beta_{ml}(Ntr^{-1}\dot{q}_m - \dot{q}) \quad (3.3)$$

where q is the vector of angular positions that describe the trajectory of the centers of mass of the link, q_m is the vector of the angular positions of the motors, K is the diagonal joint stiffness matrix that produces the vector of torques transmitted to the links, I_{ref} is the vector of the (quadrature) currents of the motors, Ntr is the diagonal matrix including the reduction ratios of the mechanical transmissions, J_m is the inertia matrix of the motor, $M(q)$ is the inertia matrix of the manipulator.

Equation (3.1) is the Lagrangian equation of the links, constituted by rigid bodies. The torque provided through the elastic elements in the mechanical system balances with: non-linear friction $f_l(\dot{q})$, viscous linear friction $\beta_l\dot{q}$, gravity torque $G(q)$, centripetal and Coriolis terms $C(q, \dot{q})\dot{q}$ and the inertial torques $M(q)\ddot{q}$.

The terms related to $C(q, \dot{q})$ can be obtained using the so called Christoffel symbols:

$$c_{ij} = \frac{1}{2} \left(\frac{\partial M_{ij}}{\partial q_k} + \frac{\partial M_{ik}}{\partial q_j} - \frac{\partial M_{jk}}{\partial q_i} \right) \quad (3.4)$$

Equation (3.2) is the dynamic equation of the motors. The torque generated in the motor (represented approximately by the product of a current reference I_{ref} by a torque constant K_t) balances with: the friction torque $\beta_m\dot{q}_m$, nonlinear friction $f_m(\dot{q}_m)$, the inertial torque that accelerates the rotating parts of the machine $J_m\ddot{q}_m$ (i.e., the driving torque), the coupling between motor and link $Ntr^{-1}\tau_l$.

Equation (3.3) is the Hooke's law. The torque is transferred because a torsion angle is created between the positions of the centers of mass and the positions of the rotors (downstream of the reduction ratio). The elastic deformation allows the torque to be transferred from the motor to the mechanical arm. In this model, unlike the original, concentrated torsion springs are considered, which represent both the elastic torsion of the transmission but also bending effects of the real arms, which lie in the plane of rotation of the arms, around the motorized axis. Therefore, they are less rigid torsional springs than those that define only the elastic characteristics of the transmission.

In general, these torsional springs are:

- non-linear (to represent backlash and angular yielding of the gearboxes)

- function of the pose q of the manipulator to represent effects of additional bending and torsion of the implemented mechanical structure, which vary with the pose and influence the angular position of the center of gravity of the structure itself, with respect to the axis of rotation.

In defining the model we assume that gyroscopic coupling effects are negligible between links and motors: it is assumed that the kinetic energy associated with the motors is only an expression of the inertia of the motors themselves and their angular velocity. This hypothesis is acceptable, in practical, when considering high gear ratios associated with the Ntr matrix.

3.2.1 Inertia matrix

The inertia matrix $M(q)$ represents how the various links of the manipulator influence each other. It is symmetric, positive definite and dependent on the robot's configuration q .

This matrix makes the system multi-variable, because it is a non-diagonal matrix in which each link is connected to all the others. If the inertia matrix were diagonal, the control of a robot could be reduced to the control of 6 axes that interact poorly or that interact only at low frequencies due, for example, to gravity torques.

However, mechanical systems are complex, that is, they have multiple inertia terms (each axis has its own inertia and mutual inertias):

- The inertias of the various axes are the diagonal entries of the inertia matrix $m_{ii}(q)$. For these terms, the torque relates the acceleration of the axis to the torque passing through the axis (which is transmitted directly by the motor).
- Mutual inertias are the off-diagonal terms of the inertia matrix $m_{ij}(q)$, $i \neq j$. They represent how the axes are coupled to each other (how the i axis influences the j axis, in a particular configuration q). These terms are the ones that contribute most to make the model a coupled multi-variable (MIMO) system. This condition is referred as "modal coupling", because the mutual influences take the form of the vibration modes of the system.

Vibrations

Any physical system with mass and elasticity can vibrate. The structure of the robot is like a short circuit for vibrations, that is, the vibrations generated on one axis reach all the other axes. The inertia matrix carries all the vibrations, in fact it is also called the modal mass matrix, where modal refers to the ways in which the structure vibrates.

The modes of vibration are linked to frequencies, which are computed as the squared root of the product between the inverse of the eigenvalues of the inertia matrix and the stiffness matrix.

$$\omega_n = \sqrt{eig(M(q_0))^{-1} \cdot K} \quad (3.5)$$

They are not fixed because they depend on $M(q_0)$, where $q = q_0$ is a joint position.

If all the axes are braked or controlled, and the system is perturbed, the structure starts to vibrate because there are masses and springs. The system returns to the point of stable equilibrium by oscillating. This is true only in a system of masses and springs in which one end of the springs (which corresponds to the driving axes, i.e., the actuators) is still.

3.3 Linearization

Linearization is the simplest way to extend linear observation techniques to nonlinear systems.

The linearization procedure with respect to a joint position $q = q_0$ allows to transform a nonlinear model into a linear one with variable parameters.

We consider the nonlinear parts of the complete model (the vector of gravitational torques, the vector of Coriolis torques, the vector of nonlinear components of the friction torques acting on the link and on the motors, the mutual inertial torques coming from the other axes) as vectors of torques, known and calculable based on of the vector q and its first derivative.

Then, in $q = q_0$, the following system of equations appears to be linear.

$$M(q_0)\ddot{q} + \beta_l\dot{q} + \tau_{ext} = \tau_l \quad (3.6)$$

$$J_m\ddot{q}_m + \beta_m\dot{q}_m + Ntr^{-1}\tau_l = K_t I_m \quad (3.7)$$

$$\tau_l = K(Ntr^{-1}q_m - q) + \beta_{ml}(Ntr^{-1}\dot{q}_m - \dot{q}) \quad (3.8)$$

where $\tau_{ext_i} = \tau_{gravity} + \tau_{coriolis} + \tau_{nonlinearfriction} + \sum_{j \neq i} m_{ij}\ddot{q}_j$.

However, as the position in the operational area varies (as the working conditions vary), the matrix $M(q_0)$ changes, so the system is Linear Parameter Varying (LPV).

3.3.1 Linear Parameter Varying (LPV) systems

Linear Parameter Varying (LPV) systems are linear dynamic systems whose mathematical description depends on parameters that change values over time:

$$\begin{cases} \dot{x}(t) = A(\rho) + B(\rho)u(t) \\ y(t) = C(\rho)x(t) \end{cases} \quad (3.9)$$

where ρ corresponds to the exogenous stationary parameter which can be time dependent. This exogenous parameter can be evaluated in real time and, consequently, all state space matrices update at each time step.

Therefore, it is a multi-step sampling process: there is a continuous sampling step for the state reconstruction and a larger sampling step in which once every N sampling steps all the matrices and the gains are updated.

An LPV system is quadratically stable, and consequently exponentially stable, if and only if there exists a quadratic Lyapunov function dependent on the parameters of the form:

$$V(x) = x^T P(\sigma)x$$

where $P(\sigma) \in \mathbb{R}^{n \times n}$ and $P(\sigma) = P(\sigma)^T > 0$ such that:

$$\dot{V}(x) = A(\rho)^T P + P A(\rho) < 0.$$

Then the system is stable for arbitrarily parameter-varying uncertainties.

3.4 Predictable torque

The torque τ_{ext} is the part of the complete dynamic model of the manipulator that is lost by locally linearizing the system. It can be divided into two contributions:

$$\tau_{ext} = \tau_{predictable} + \tau_d \quad (3.10)$$

where:

- $\tau_{predictable}$ is the part that can be calculated based on the dynamic model of the manipulator. It is deterministic and known.
- τ_d is the unknown part to be reconstructed (it is included in the state of the observer).

The prediction torque $\tau_{predictable}$ is a sort of feedforward that allows to take into account the parts that are not present and it gives robustness to the observer. It is defined as:

$$\tau_{predictable} = C(q, \dot{q})\dot{q} + G(q) + f_{nl}(\dot{q}) + [M(q) - \text{diag}(m_{ii}(q))]\ddot{q} \quad (3.11)$$

where q, \dot{q}, \ddot{q} are the target estimates, $f_{nl}(\dot{q})$ include any nonlinear friction components.

We cannot take directly the targets because these machines (but in general all control systems), if well controlled, have a delay (of about 20 ms). It means that reality is misaligned with respect to the target and in carrying out the reconstruction of the torques acting on the link we must respect the signal transfer times (if the signals are not synchronized, apparent disturbances arise). An example of delay between the target and the real joint position is represented in Figure 3.2.

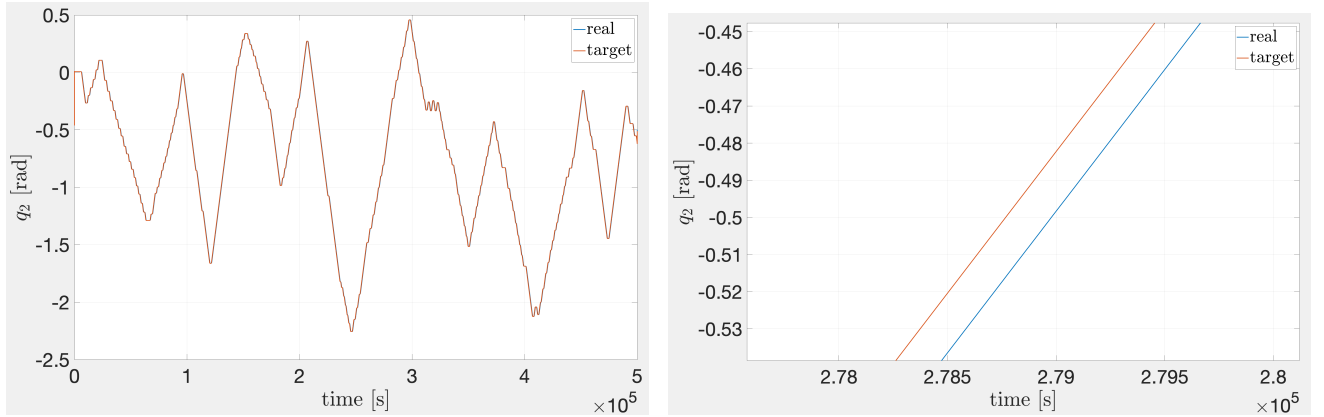


Figure 3.2. Target and the real joint position and relative zoom (delay)

Reducing the terms of $\tau_{predictable}$ to exogenous and calculable input signals to the models is one acceptable approximation and helps to reduce the model to the form of a linear system with variable parameters (LPV).

The same thing cannot be done for mutual inertial terms. The main reasons are:

- The system, as a whole, is MIMO and this structure is mainly linked to non-diagonal inertia matrix $M(q)$.
- Accelerations \ddot{q}_i emphasize the high frequency response and are very different from estimates that can be obtained starting from the theoretical trajectories planned by the control of manipulator. This is especially true when executing highly dynamic trajectories, characterized by significant medium and high frequency components.
- Theoretical trajectories planned by the manipulator control are produced by a rigid machine model. The accelerations, which characterize them, never contain vibrations or oscillations. The accelerations \ddot{q}_i of the actual manipulator are produced, starting from the energy associated with the trajectory to be followed, by the excitation of the vibration modes of the mechanical structure, which are characterized by low frequencies and very small damping.
- In general, therefore, \ddot{q}_i can express low-frequency, persistent oscillations of significant amplitude and little damping that a filtered target acceleration will never be able to predict.

For these reasons the terms $\sum_{i \neq 2} m_{2i}(q) \cdot \ddot{q}_i$ must be traced back to the sum of two contributions:

$$\sum_{i \neq 2} m_{2i}(q) \cdot \ddot{q}_i = \sum_{i \neq 2} m_{2i}(q) \cdot \delta \ddot{q}_i + \sum_{i \neq 2} m_{2i}(q) \cdot \tilde{\ddot{q}}_i \quad (3.12)$$

The term $\sum_{i \neq 2} m_{2i}(q) \cdot \tilde{\ddot{q}}_i$ represents the low frequency, “rigid machine” part of the mutual inertial torque and can be obtained starting from the planned theoretical trajectories, using the same filters defined before. These contributions can also be considered as exogenous input signals to the observer’s model.

The term $\sum_{i \neq 2} m_{2i}(q) \cdot \delta \ddot{q}_i$ represents that very significant part of the mutual inertial torques, linked to the modes of vibration of the structure, which cannot be traced back in any way to the planned rigid machine trajectories and must be represented within the observer model. The way of representing this term of the model differentiates the various typologies of independent joint observers, which are the subject of development and testing within the scope of the thesis.

Gravity compensation

To simplify development and testing work, without taking away the generality and meaning of the work carried out, operating conditions of a single axis are considered, specifically axis 2, in conditions in which the other axes are controlled in a planned trajectory at constant position.

Therefore, the predictable torque acting on link 2 is made up of:

- Gravity
- Inertial torque: apart from axis 3, which is more influenced by the movement of axis 2, it is assumed that the other axes do not vibrate, and therefore they do not have an inertial torque.
- Coriolis terms: they tend to be naturally neglected because only axis 2 moves.

Therefore, only the gravity components need to be calculated (gravity is transferred from a disturbance acting on the motor to a disturbance acting on the center of mass of the link).

Gravity can be estimated using a sinusoidal function of the position, which does not depend on the direction of rotation:

$$\alpha \cdot \sin(\cdot) + \beta \cdot \cos(\cdot)$$

The argument of sine and cosine are linked to the angular position of the axis 2 (we take into account that we measure it at the level of the motor current, but then we make it act downstream of the transmission, therefore directly on the center of mass).

```

1 function grav = grav_est(pos,cur,Kt,Ts)
2 vel = deriva(pos,Ts);
3 acc = deriva(vel,Ts);
4 % Indexes for addressing
5 VelIdx = find( ( abs( vel(:,2) ) > 2 ) & ( abs( acc(:,2) ) < 60 ) );
6 % Regression matrix
7 A = [ sin( pos(:,2) ), cos( pos(:,2) ) ];
8 % Regressor
9 y = Kt*cur(:,2);
10
11 X_dyn = pinv(A(VelIdx,:))*y(VelIdx,:);
12 grav = A*X_dyn;
13 end

```

The gravity torque can be computed using the dynamic model for a rigid machine (as if it were an exogenous term that is not conditioned by the system, neither at the control level nor at the observer level). Since gravity depends on the position, the gravitational torque acts at a very low frequency (a frequency range that is separate from vibrations). Therefore the presence of vibrations does not cause problems.

3.5 Discretization

State estimation and control algorithms are almost always implemented in digital electronics. This often requires a transformation of continuous-time dynamics to discrete-time dynamics. The digital world is not an extension of the analog world, but it is a subspace: there are things from the analog world that are not portable into digital.

A common situation in computer control is that the D-A converter is a filter that keeps the analog signal constant until a new conversion is commanded. This is often called a zero-order-hold (ZOH) circuit. Because the control signal is discontinuous, it is necessary to specify its behavior at the discontinuities. The convention that the signal is continuous from the right is adopted [17].

Let's consider a linear system, with multiple outputs and inputs (MIMO), strictly proper ($D = 0$), without transport delays:

$$\begin{aligned} \dot{x} &= A \cdot x + B \cdot u \\ y &= C \cdot x \end{aligned}$$

It corresponds to the algebraic expression that uses the Laplace operator:

$$\begin{aligned} s \cdot X(s) &= A \cdot X(s) + B \cdot U(s) \\ Y(s) &= C \cdot X(s) \end{aligned}$$

We obtain the following expressions in discrete time:

$$\begin{aligned} x(k+1) &= A^* \cdot x(k) + B^* \cdot u(k) \\ y(k) &= C^* \cdot x(k) \end{aligned}$$

The discretization formulas are as follows:

$$A^* = e^{A \cdot T_s} \quad (3.13)$$

$$B^* = A^{-1} \cdot (e^{A \cdot T_s} - I) \cdot B \quad (3.14)$$

$$C^* = C \quad (3.15)$$

Consider the Taylor series expansion of the exponential matrix:

$$A^* = I + A \cdot T_s + \frac{1}{2} A^2 \cdot T_s^2 + \dots \quad (3.16)$$

$$B^* = \left(T_s + \frac{1}{2} A \cdot T_s^2 + \dots \right) \cdot B \quad (3.17)$$

If we consider only the terms in T_s of power 1 of the expansion, we find the Euler discretization formulas. Therefore, the commonly proposed discretization formulas (forward Euler, backward rectangular, bilinear transform) are to be considered approximate and not exact.

Only the discretization through the calculation of the exponential matrix provides an exact representation of the dynamics of the continuous system, transformed into its digital representation. This is particularly true if we consider systems of equations characterized by complex eigenvalues (poles) and transmission zeros, with reduced damping: an approximate discretization can give a mismatched representation of the frequencies and dampings of the poles and zeros of the system (as a consequence, the digital system may vibrate at a slightly different frequency than the analog one). Therefore, in the representation of non-rigid electromechanical systems, the use of the exponential matrix is recommended. In many cases, the use of the first 4-5 terms of the Taylor series expansion guarantees a sufficiently faithful representation of the dynamics of the analog model in continuous time.

3.6 Observer

The model reduced to the double pendulum (axis 2 and 3) is considered, analytically eliminating the other 4 axes considered as braked and ideally rigid (they have no elastic contributions). Axis 2 is considered the observed system, and axis 3 is present as additional dynamics. For axis 3 the motor is braked but the elastic dynamics of link 3 is present (the link is not braked). When axis 3 is energized by the current of 2, the unbraked part of the dynamics of link 3 manifests itself in the form of vibrations that impact the dynamics of axis 2.

The model can be divided into two blocks, connected, in feedback, by mutual inertial torques (as shown in Figure 3.3):

1. The nominal part of the model coincides with the modeled dynamics of the center of mass of the robotic arm, referred to the rotation axis 2.
2. The higher order part is defined as the “uncertainty function”.

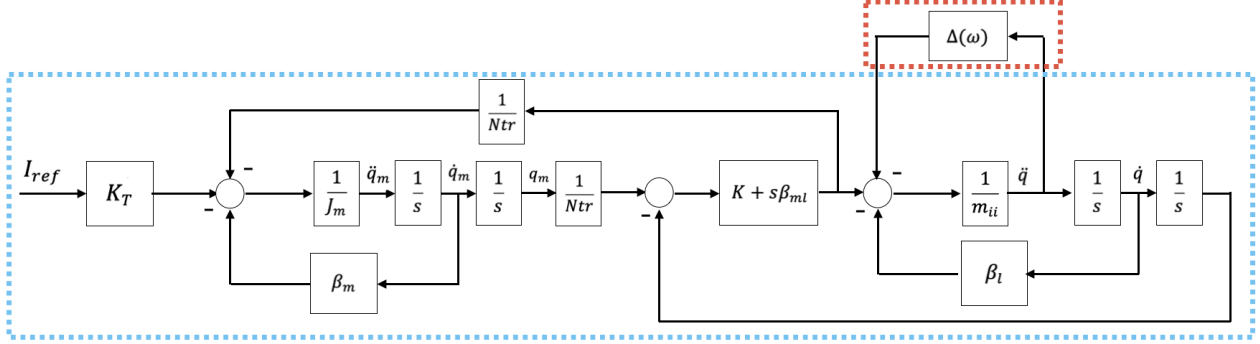


Figure 3.3. Observer structure

The mutual inertial action, which introduces higher order modes of vibration, can be represented, in the nominal model, as an external torque disturbance $\Delta(\omega)$ which acts on the torque balance at the output of the elastic joint. The $\Delta(\omega)$ signal changes the nature of the system from an isolated and single-variable system to a multi-variable system.

The $\Delta(\omega)$ signal is reconstructed by introducing additional state variables that are observable, but not controllable (i.e., it is not possible to assign the dynamics of the center of mass).

The introduction and management of these variables:

- allows a significant reduction in model order
- maintains high accuracy in the reconstruction of the angular position and angular velocity of the center of mass.

The various types of observers are distinguished by the way this signal $\Delta(\omega)$ is modeled.

3.6.1 6-state observer

State-space representation

To have a state-space representation, starting from the Spong’s model, we must obtain the strictly proper ($D = 0$) system of equations:

$$\begin{aligned}\dot{x} &= Ax + Bu + B_1\tau_{predictable} \\ y &= Cx\end{aligned}$$

Note that the predictable torque is also taken into account as a second input to the model, as discussed in Section 3.4.

Let’s consider:

- $u = I_{ref_2}$, where I_{ref_2} is the joint quadrature current induced by the motor of axis 2. Only axis 2 is powered, axis 3 is considered a parasitic (driven) axis.
- $x = [\dot{q}_2 \ \dot{q}_3 \ \dot{q}_{2m} \ q_2 \ q_3 \ q_{2m}]$. The degrees of freedom that correspond to the braked actuator (axis 3 motor) are eliminated.
- $y = q_{2m}$.

Then, combining the equations (3.1), (3.2), (3.3) together with the definitions of state, input and output, we obtain the following (continuous time) state space matrices:

$$A = \begin{bmatrix} \frac{-M(3,3)\beta_{lml}(2,2)}{\det M} & \frac{M(2,3)\beta_{lml}(3,3)}{\det M} & \frac{M(3,3)\beta_{ml}(2,2)}{Ntr(2,2)\cdot\det M} & \frac{-M(3,3)K(2,2)}{\det M} & \frac{M(2,3)K(3,3)}{\det M} & \frac{M(3,3)K(2,2)}{Ntr(2,2)\cdot\det M} \\ \frac{M(3,2)\beta_{lml}(2,2)}{\det M} & \frac{-M(2,2)\beta_{lml}(3,3)}{\det M} & \frac{-M(3,2)\beta_{ml}(2,2)}{Ntr(2,2)\cdot\det M} & \frac{M(3,2)K(2,2)}{\det M} & \frac{-M(2,2)K(3,3)}{\det M} & \frac{-M(3,2)K(2,2)}{Ntr(2,2)\cdot\det M} \\ \frac{\beta_{ml}(2,2)}{Ntr(2,2)J_m(2,2)} & 0 & \frac{\beta_m(2,2)+\beta_{ml}(2,2)\cdot Ntr(2,2)^{-2}}{J_m(2,2)} & \frac{K(2,2)}{Ntr(2,2)J_m(2,2)} & 0 & \frac{-K(2,2)}{Ntr(2,2)^2J_m(2,2)} \\ 1 & 0 & 0 & 0 & 0 & 0 \\ 0 & 1 & 0 & 0 & 0 & 0 \\ 0 & 0 & 1 & 0 & 0 & 0 \end{bmatrix} \quad (3.18)$$

$$B = \begin{bmatrix} 0 \\ 0 \\ \frac{K_t(2,2)}{J_m(2,2)} \\ 0 \\ 0 \\ 0 \end{bmatrix} \quad (3.19)$$

$$B_1 = \begin{bmatrix} -\frac{1}{M(2,2)} \\ 0 \\ 0 \\ 0 \\ 0 \\ 0 \end{bmatrix} \quad (3.20)$$

$$C = [0 \ 0 \ 0 \ 0 \ 0 \ 1] \quad (3.21)$$

where $\beta_{lml}(i, i) = \beta_l(i, i) + \beta_{ml}(i, i)$ and $\det M = M(2,2)M(3,3) - M(2,3)M(3,2)$.

Frequency analysis

The transfer function between the current reference that we send to the motor of axis 2 and the speed of the motor of axis 2 has the form shown in Figure 3.4.

The trend can be divided into 3 parts:

1. Low frequency part: there is always a mechanical pole that drops as -20 dB/dec. It is a function of the overall friction and total inertia $\frac{K_t}{sJ_{tot}}$, $J_{tot} = J_m + \frac{J_l}{Ntr^2}$. The dynamics of the motor dominates.
2. Intermediate part (between 20 and 30 Hz): transmission zeros and resonant poles alternate in this range. This behavior is typical of non-rigid systems and it represents the mutual interaction between the axes. In this part, the dynamics of the external system dominates. Therefore, there are frequency ranges in which the interaction between the axes has greater effects.

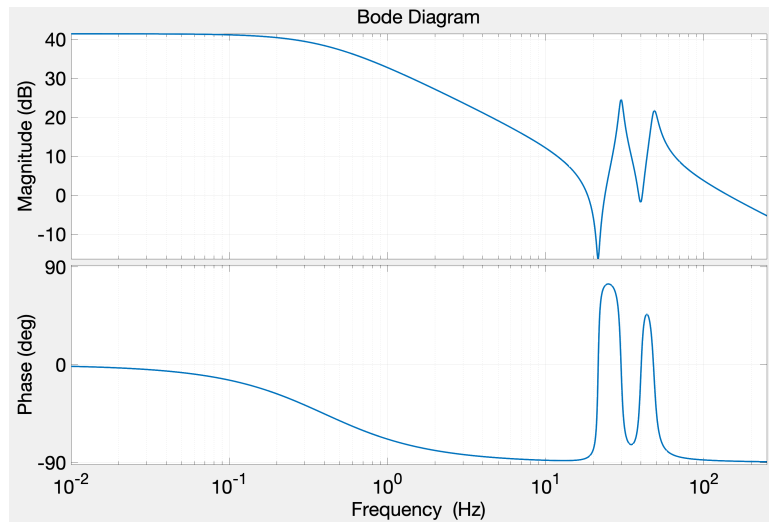


Figure 3.4. Plant transfer function

3. High frequency part: this frequency range is defined by the threshold represented by the ratio $\frac{K_t}{sJ_m}$.

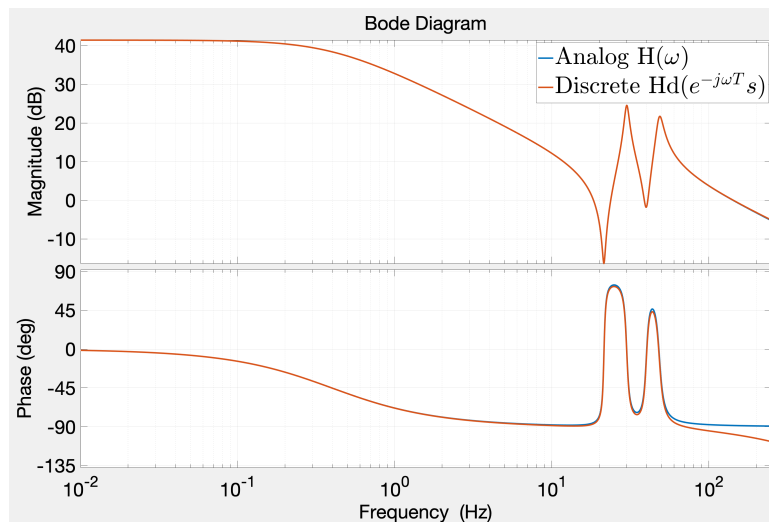


Figure 3.5. Model discretization

Figure 3.5 shows the discretization of the model under the hypothesis of:

1. synchronous sampling step
2. zero transport delays: we assume that between the CPU where the speed control that produces the requested current runs and the drive there is an instantaneous direct line (in reality this is not the case)

3. zero-order-hold filter.

The phase loss of the discrete system is due to the presence of the zero order hold filter, which introduces a time delay of approximately $\frac{T_s}{2}$. A sampling step $T_s = 400\mu s$ is used for the discretization.

3.6.2 5-state observer

State-space representation

Starting from the linearized Spong's model, we must obtain the system of equations:

$$\begin{aligned}\dot{x} &= Ax + Bu + B_1\tau_{predictable} \\ y &= Cx\end{aligned}$$

Let's consider:

- $u = I_{ref2}$, where I_{ref2} is the joint quadrature current induced by the motor of axis 2.
- $x = [\dot{q}_2 \quad \dot{q}_{2m} \quad q_2 \quad q_{2m} \quad \tau_{ext}]$. Only axis 2 is considered as an isolated system. The additional state τ_{ext} represents all the torques acting on the arm's center of mass that are not explicitly modeled in the observer.
- $y = q_{2m}$.

Then, combining the equations (3.1), (3.2), (3.3) together with the definitions of state, input and output, we obtain the following (continuous time) state space matrices:

$$A = \begin{bmatrix} \frac{-\beta_l(2,2) - \beta_{ml}(2,2)}{M(2,2)} & \frac{\beta_{ml}(2,2)}{Ntr(2,2)M(2,2)} & \frac{-K(2,2)}{M(2,2)} & \frac{K(2,2)}{Ntr(2,2)M(2,2)} & -\frac{1}{M(2,2)} \\ \frac{\beta_{ml}(2,2)}{Ntr(2,2)J_m(2,2)} & \frac{-\beta_m(2,2) - \beta_{ml}(2,2) \cdot Ntr(2,2)^{-2}}{J_m(2,2)} & \frac{K(2,2)}{Ntr(2,2)J_m(2,2)} & \frac{-K(2,2)}{Ntr(2,2)^2 J_m(2,2)} & 0 \\ 1 & 0 & 0 & 0 & 0 \\ 0 & 1 & 0 & 0 & 0 \\ 0 & 0 & 0 & 0 & 0 \end{bmatrix} \quad (3.22)$$

$$B = \begin{bmatrix} 0 \\ \frac{K_t(2,2)}{J_m(2,2)} \\ 0 \\ 0 \\ 0 \end{bmatrix} \quad (3.23)$$

$$B_1 = \begin{bmatrix} -\frac{1}{M(2,2)} \\ 0 \\ 0 \\ 0 \\ 0 \end{bmatrix} \quad (3.24)$$

$$C = [0 \quad 0 \quad 0 \quad 1 \quad 0] \quad (3.25)$$

Frequency analysis

Figure 3.6 shows the response of axis 2 as an isolated system. In this case there is only one anti-resonance frequency. The transmission zero shifts slightly with respect to the previous case. It is as if axis 2 lost part of its load inertia.

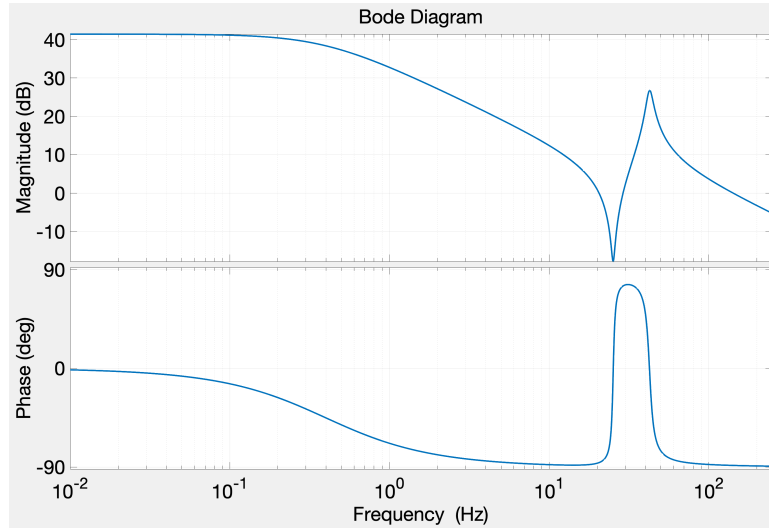


Figure 3.6. 5-state observer transfer function

3.6.3 4-state observer

State-space representation

Starting from the linearized Spong's model, we must obtain the system of equations:

$$\begin{aligned}\dot{x} &= Ax + Bu + B_1\tau_{predictable} \\ y &= Cx\end{aligned}$$

Let's consider:

- $u = I_{ref2}$, where I_{ref2} is the joint quadrature current induced by the motor of axis 2.
- $x = [\dot{q}_2 \quad \dot{q}_{2m} \quad q_2 \quad q_{2m}]$: the model does not include inertial torques. It is the simplest model in which axis 2 is alone and the dynamics of the other axes simply add a load inertia to axis 2.
- $y = q_{2m}$.

Then, we obtain the following (continuous time) state space matrices:

$$A = \begin{bmatrix} \frac{-\beta_l(2,2) - \beta_{ml}(2,2)}{M(2,2)} & \frac{\beta_{ml}(2,2)}{Ntr(2,2)M(2,2)} & \frac{-K(2,2)}{M(2,2)} & \frac{K(2,2)}{Ntr(2,2)M(2,2)} & -\frac{1}{M(2,2)} \\ \frac{\beta_{ml}(2,2)}{Ntr(2,2)J_m(2,2)} & \frac{-\beta_m(2,2) - \beta_{ml}(2,2)Ntr(2,2)^{-2}}{J_m(2,2)} & \frac{K(2,2)}{Ntr(2,2)J_m(2,2)} & \frac{-K(2,2)}{Ntr(2,2)^2J_m(2,2)} & 0 \\ 1 & 0 & 0 & 0 & 0 \\ 0 & 1 & 0 & 0 & 0 \end{bmatrix} \quad (3.26)$$

$$B = \begin{bmatrix} 0 \\ \frac{K_t(2,2)}{J_m(2,2)} \\ 0 \\ 0 \end{bmatrix} \quad (3.27)$$

$$B_1 = \begin{bmatrix} -\frac{1}{M(2,2)} \\ 0 \\ 0 \\ 0 \end{bmatrix} \quad (3.28)$$

$$C = [0 \ 0 \ 0 \ 1] \quad (3.29)$$

3.6.4 7-state observer

Instead of simply adding an observable state, the order of the system is increased, so that there is a subsystem that is powered by an unspecified input signal. The additional state is not simply a nominally constant state but is powered by its own dynamic block (a filter that is synchronized in the frequency range in which the interaction between axes 2 and 3 is expressed).

Various types of filters have been tried, but the only one that makes the overall system completely observable is a resonant low pass filter. Figure 3.7 represents it.

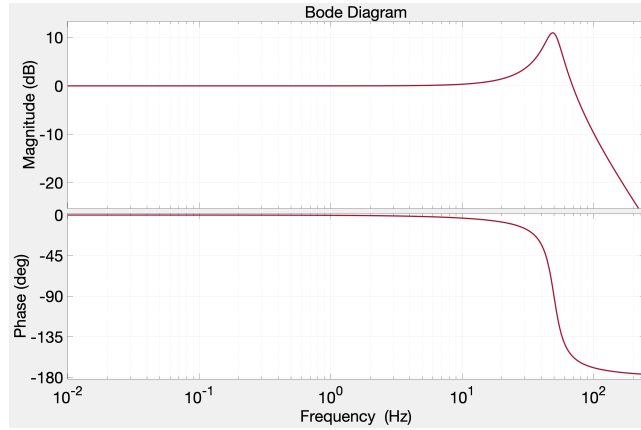


Figure 3.7. Resonant low pass filter

With a model of this type it is possible to reconstruct the action of static friction and gravity which operate at low frequency separately from the mutual inertial torques which are related to accelerations (have medium-high frequency emphasis).

This way the state becomes bigger and more difficult to manage (there are more gains to calibrate) but it is much more focused. We don't always have the opportunity to know the dynamics of the robot so well and we would like to have observers who, having a reduced set of information on the single axis, are able to reconstruct the relationships with the other axes well.

State-space representation

To have a state-space representation, starting from the linearized Spong's model, we must obtain the system of equations:

$$\begin{aligned} \dot{x} &= Ax + Bu + B_1\tau_{predictable} \\ y &= Cx + Du \end{aligned}$$

Let's consider:

- $u = I_{ref_2}$, where I_{ref_2} is the joint quadrature current induced by the motor of axis 2.
- $x = [\dot{q}_2 \quad \dot{q}_{2m} \quad q_2 \quad q_{2m} \quad \tau_{ext} \quad \dot{\tau}_{ext} \quad x_7]$.
- $y = q_{2m}$.
- The transfer function of the filter in the Figure 3.7 is of the type represented in (3.30).

$$H(s) = \frac{X_5(s)}{X_7(s)} = \frac{\omega_n^2}{1 + 2\zeta\omega_n s + \omega_n^2 s^2} \quad (3.30)$$

Then, we obtain the following (continuous time) state space matrices:

$$A = \begin{bmatrix} \frac{-\beta_l(2,2) - \beta_{ml}(2,2)}{M(2,2)} & \frac{\beta_{ml}(2,2)}{Ntr(2,2)M(2,2)} & \frac{-K(2,2)}{M(2,2)} & \frac{K(2,2)}{Ntr(2,2)M(2,2)} & -\frac{1}{M(2,2)} & 0 & 0 \\ \frac{\beta_{ml}(2,2)}{Ntr(2,2)J_m(2,2)} & \frac{-\beta_m(2,2) - \beta_{ml}(2,2) \cdot Ntr(2,2)^{-2}}{J_m(2,2)} & \frac{K(2,2)}{Ntr(2,2)J_m(2,2)} & \frac{-K(2,2)}{Ntr(2,2)^2 J_m(2,2)} & 0 & 0 & 0 \\ 1 & 0 & 0 & 0 & 0 & 0 & 0 \\ 0 & 1 & 0 & 0 & 0 & 0 & 0 \\ 0 & 0 & 0 & 0 & 0 & 1 & 0 \\ 0 & 0 & 0 & 0 & -\omega_n^2 & -2\zeta\omega_n & \omega_n^2 \\ 0 & 0 & 0 & 0 & 0 & 0 & 0 \end{bmatrix} \quad (3.31)$$

$$B = \begin{bmatrix} 0 \\ \frac{K_t(2,2)}{J_m(2,2)} \\ 0 \\ 0 \\ 0 \\ 0 \\ 0 \end{bmatrix} \quad (3.32)$$

$$B_1 = \begin{bmatrix} -\frac{1}{M(2,2)} \\ 0 \\ 0 \\ 0 \\ 0 \\ 0 \\ 0 \end{bmatrix} \quad (3.33)$$

$$C = [0 \ 0 \ 0 \ 1 \ 0 \ 0 \ 0] \quad (3.34)$$

3.7 Friction

Friction appears in the expression of Spong’s model in (3.2) added to the torque transmitted by the motor to the mechanical system (the arm) in producing the driving torque:

$$\tau_{mot_2} = -\beta_{m2} \cdot \dot{q}_{m2} - f_{m2} - \frac{\tau_{l2}}{Ntr_{22}} + K_{t2} \cdot I_{ref_2} \quad (3.35)$$

While the predictable and gravity torques act downstream of the elastic elements (downstream of the transmission), friction is considered for convenience as acting on the transmission, and therefore essentially on the motor.

If we cannot distinguish between torque transmitted to the link and friction, it is not possible to reconstruct the operating state of the link, starting from the knowledge of the motor current and the motor position measurement alone. The presence of friction is interpreted as a trend of the reconstructed state, which however is fictitious. From this arises the need for accurate modeling of friction, in particular, of the friction acting on the motor.

The nonlinear friction components are only partially related to the Coulomb friction phenomenon, which can be represented using “static”, arctangent (or sigmoid) functions of the rotation velocity:

$$F = f_c \text{sign}(\dot{q}_m) + f_v \dot{q}_m \quad (3.36)$$

where f_c and f_v are two parameters representing Coulomb friction and viscous friction, respectively.

The sign function is discontinuous and mathematical discontinuities should not be introduced into physical systems. It must be approximated with arctangents or sigmoids, because they are continuous functions with continuous derivatives but generate transition conditions.

The viscous friction components are represented in the linear and explicit part of the model but are characterized by uncertain parameters, which must be identified experimentally and, possibly, in an adaptive way, to track the inevitable variations with temperature, wear of the machine, conditions operating dynamics (see Section 3.8).

3.7.1 Open chain simulation of friction

This method is constituted by a friction observer, in the sense that it simulates friction: a predictive model of the Coulomb friction which subtracts from the reference current is added in the observer. It is called a detrender. Adding this prediction in feedforward, the observer can know that a part of the

currents that the regulator gives to axis 2 do not serve to change the internal state of the axis, but also serve to balance the friction torques: it is a model closer to reality.

Arctangent works very well together with viscous friction, if we need to compensate for nonlinear and linear frictions when the system is at medium-high speed. The presence of Stribeck friction (a friction that occurs when the axis begins to rotate at a very low speed) or sliding friction (mesh friction) cannot be traced back to simple models of Coulomb friction.

Furthermore, static friction torques highlight the existence of an internal state of friction which introduces the need for a dynamic and non-static model, as a function of speed. Very often robots have some axes that remain stationary or have axes that reverse their motion several times during a cartesian movement or move very slowly. In those speed regimes these friction models are no longer valid. For these reasons it is appropriate to model friction using advanced models such as LU-GRE [18], Dahl [19] or Maxwell slip.

3.7.2 Synthesis of a pole placement regulator

Alternatively, during the thesis, we intend to experiment the use of an additional observer, defined as an input disturbance observer, to model friction as an uncertain input signal to the motor. The dynamics of friction can be represented as a non-linear counter-reaction, of the proportional-integral type, between the rotation speed and a sum node with the driving torque. The action of friction tends to brake the motor, so it subtracts torque from the motor (it tends to oppose the movement).

The disturbance observer was built as a synthesis of a pole placement regulator, which produces a non-measurable signal at the motor input that is used to reconstruct the friction components that are not immediately estimated and the missing part of the dynamics in the observer.

In [17], it is explained that the control of the state variables is equivalent to the control in polynomial form. A control of this type, compared to a PI (Proportional-Integral), has a higher implementation cost but:

- It presents a trend with low frequency integrative action on the error position (dimensionally almost a rotation velocity). It should allow static and non-linear frictions to be well represented (disturbances characterized by an implicit regulation loop, proportional integral, nonlinear, on the rotation speed).
- It allows a better estimate of input disturbances, reducing their effect on the estimate of states that are not immediately measurable.
- It fixes the position of the poles of the internal state observer, using cancellation zeros.
- Due to the way this regulator is made, it tends not to influence the poles of the internal observer. The result is greater robustness of stability. An external PI type regulator shifts the assigned poles of the internal observer and tends to change the dynamics of the overall closed loop system (according to control theory in the case of nested rings, the stronger regulator is the outer one, called high priority control).

The two observers must work in separate bands: one part deals with friction and one with state estimation (inertial torques, rotation speed). In reality, they are overlapped in band (this arises from the fact that in analogue systems there is no digital separation): by continuously varying the band of the

disturbance observer, it is possible to better isolate certain components or better intercept components that are not torque disturbances.

The disturbance observer must be slow enough not to disturb the internal part, strong enough to be able to reconstruct the low frequency dynamics of the friction. If the disturbance observer is too strong the motor position is reconstructed well but the link speed is not; instead, if the friction has too fast dynamics, its compensation is partial. This is a tradeoff that we must accept.

To construct the pole placement regulator, we need to study the transfer function between the model input and the observer's estimate error. Based on that, we design a further control loop that imposes an integrative action on the estimate error, that helps to better correct the effects of friction.

Therefore, we use the estimate error twice:

- A first time to close the innermost part of the observer
- A second time by adding an integrative action to try to compensate for the effects of friction.

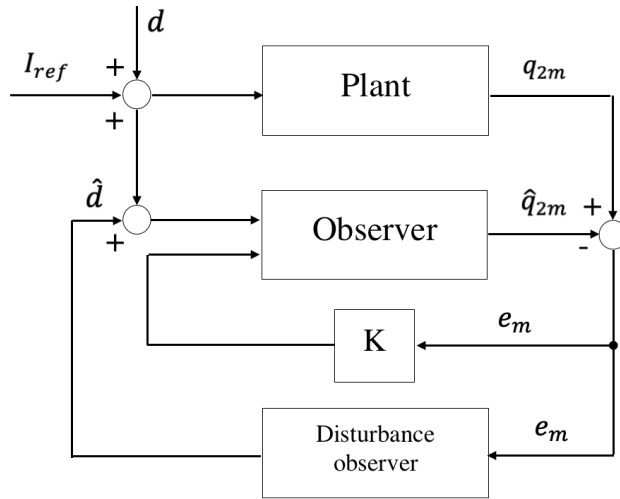


Figure 3.8. Complete scheme with disturbance observer

From the scheme in Figure 3.8, we can see how the observer's input is no longer the entire current that is given to the drive, but only the remaining part, after subtracting the current that balances the friction.

Discrete time control via pole placement algebraic approach

Consider the 1dof architecture in Figure 3.9, where $C(z) = \frac{S(z)}{R(z)}$ is the digital controller and $G(z) = \frac{B(z)}{A(z)}$ includes the actuator and the plant.

Assume that: $A(z), B(z)$ are coprime (i.e., they have no common roots), $G(z)$ is strictly proper (i.e., $\deg(A(z)) = m > \deg(B(z))$), $A(z)$ is monic (i.e., unitary leading coefficient), $B(z)$ has no roots at $z = 1$, $C(z)$ is proper (i.e., $\deg(R(z)) = v \geq \deg(S(z))$).

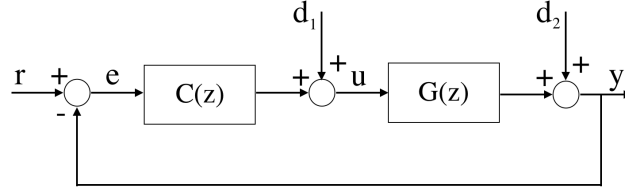


Figure 3.9. 1dof architecture

The transfer function between the reference and the output is given by:

$$W(z) = \frac{G(z)C(z)}{1 + G(z)C(z)} = \frac{B(z)S(z)}{A(z)R(z) + B(z)S(z)} = \frac{B_m(z)}{A_m(z)} \quad (3.37)$$

The problem is to design a controller $C(z)$ to place the roots of the closed loop characteristic polynomial $A_m(z)$ at given arbitrary locations. The problem can be solved by imposing:

$$A(z)R(z) + B(z)S(z) = A_m(z) \quad (3.38)$$

The equation (3.38) is known as Diophantine equation.

Pole-placement design reduces to the algebraic problem of finding polynomials $R(z)$ and $S(z)$ that satisfy (3.38) for given $A(z)$, $B(z)$ and $A_m(z)$. The problem can be always solved if the polynomials $A(z)$ and $B(z)$ do not have common factors.

Collecting the poles at $z = 1$, $G(z)$ and $C(z)$ are expressed as:

$$G(z) = \frac{B(z)}{(z-1)^{l_1}A'(z)}, C(z) = \frac{S(z)}{(z-1)^{l_2}R'(z)} \quad (3.39)$$

where $\deg(A'(z)) = m - l_1$, $\deg(R'(z)) = v - l_2$.

The closed loop transfer function from r to y becomes:

$$W(z) = \frac{B(z)S(z)}{(z-1)^l A'(z)R'(z) + B(z)S(z)} = \frac{B_m(z)}{A_m(z)}, l = l_1 + l_2 \quad (3.40)$$

The equation becomes:

$$(z-1)^l A'(z)R'(z) + B(z)S(z) = A_m(z) \quad (3.41)$$

where $(z-1)^l A'(z)$ and $B(z)$ are coprime.

Zero-pole cancellations

To simplify the main closed loop dynamics, stable zero-pole cancellations between $G(z)$ and $C(z)$ can be imposed:

$$G(z) = \frac{B^+(z)B^-(z)}{(z-1)^{l_1}A^+(z)A^-(z)} \quad (3.42)$$

where $B^+(z)$ and $A^+(z)$ are the “stable” factors that can be cancelled.

To cancel $A^+(z)$ and $B^+(z)$, $R(z)$ and $S(z)$ must be of the form:

$$R(z) = (z - 1)^{l_2} B^+(z) R'(z), S(z) = A^+(z) S'(z) \quad (3.43)$$

The controller then becomes:

$$C(z) = \frac{S(z)}{R(z)} = \frac{A^+(z) S'(z)}{(z - 1)^{l_2} B^+(z) R'(z)} \quad (3.44)$$

The diophantine equation to be solved is:

$$(z - 1)^l A^-(z) R'(z) + B^-(z) S'(z) = A_m(z)$$

In the considered case, the characteristics of the synthesis (pole placement by cancellation of the dominant poles) are:

1. cancel all the dominant poles: $A^+(z) = A(z)$, $A^-(z) = 1$
2. keep the zeros in the output: $B^+(z) = 1$, $B^-(z) = B(z)$
3. imposes the poles of the closed chain as denominator: $A_m(z) = 1 + C(z)$
4. presence of an integral action: $l_2 = 1$
5. no poles at $z = 1$ in the plant: $l_1 = 0$.

Combining these information, the diophantine equation to be solved is:

$$(z - 1) R'(z) + B(z) S'(z) = 1 + C(z) \quad (3.45)$$

The feasibility of the input disturbance observer can be affected by the model used by the observer that reconstructs the complete state of the axis.

3.8 Estimation of friction parameters

The goal of this part is to obtain numerical values that are descriptive of the axes we are considering (2 and 3) to have an estimation of the friction parameters.

Estimating friction parameters is complicated. The problem is that the values change with position, time and temperature. Friction alone could not be measured: if I want to estimate the friction I must also estimate the inertial torque (the torque component that the motor gives to accelerate/decelerate) and the gravity component (axes 2 and 3 are immersed in the gravitational field).

Friction is very rich in components and when we model it we always tend to give a simplified representation. Here we try to take at least the following two components into account:

1. Those on the rotation axis linked to the ball bearings: this friction arises from the fact that the spheres are crushed slightly at the poles against the groove of the raceway. A ball bearing is composed by a stator part and a rotor part. The inner ring has a rolling groove with a spherical profile. It is made rotoric by the fact that there are spheres that are kept at an equal distance and that roll inside the grooves. The external stator part is smooth on one side and on the other it has a track (semi-spherical profile groove).

- The rubbing friction that is absorbed by the motor: it does not develop in the bearings but directly on the gear teeth. The gears' teeth are like small beams and one gear has teeth that penetrate the toothed profile of the other gear: when sliding, the beams rub against each other. In the rubbing there is a friction of contact which depends on the force normal to the surfaces that rub (it is proportional to the torque that the gear is transmitting). This friction is called mesh friction.

There is no place in the observer to represent these friction components: they are part of all those things that act as disturbances in the reconstruction of the state.

Movement program

A movement program is made so that the considered axis (2 or 3) cycles back and forth at a constant speed (it goes from negative to positive stroke).

To carry out a data consistency analysis, three movement programs are tested: two for axis 2 (one with axis 3 extended and one with axis 3 folded) and one for axis 3 (the position of 2 is chosen to allow the travel of 3 to be extended as much as possible).

At the beginning, the program reduces acceleration and deceleration, because if they are excessive they create the presence of vibration (the measurement of friction in the presence of vibrations is not good). It sets the local speed overrides to 100%, then operates on the general machine overrides (it reduces acceleration and deceleration to 40%).

To measure friction well, the axis must travel a fairly significant angular section at constant speed to obtain a trapezoidal speed profile: for very fast manipulators, if the speed is maximum and the acceleration is reduced to 40%, a triangular profile is obtained (it accelerates, reaches a maximum value and then decelerates) and the friction cannot be measured. For this reason, a speed reduction factor is introduced. Figure 3.10 shows an example of trapezoidal and triangular speed profiles.

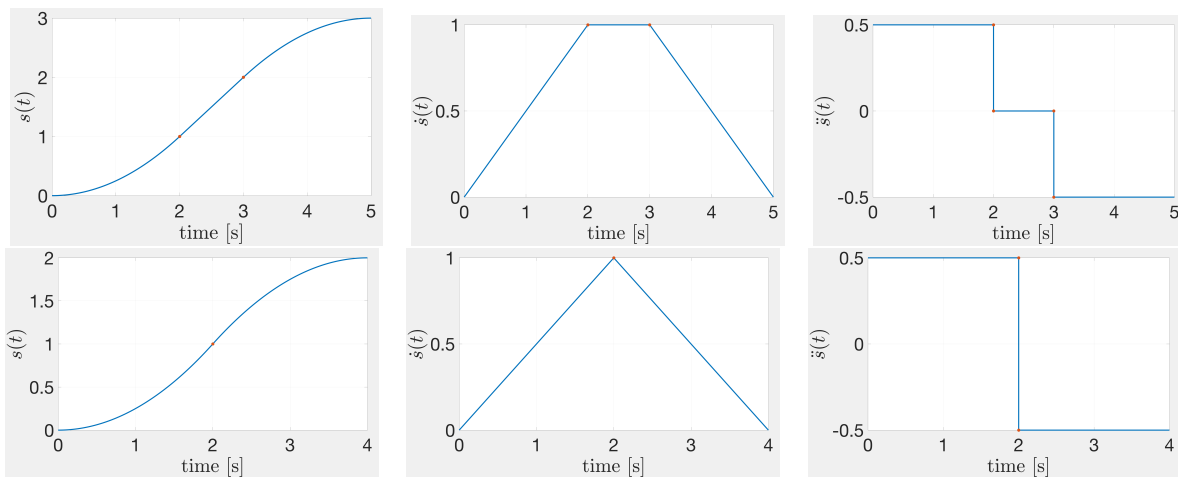


Figure 3.10. Trapezoidal and triangular speed profile

The initial part lasts 60 seconds and serves to warm up the transmission. Then a measurement cycle starts which is repeated 5 times by changing the speed.

First method of estimation

The first method of estimation provides a complete regressor, which serves to derive not only the friction terms but also the gravity, the overall inertia in those conditions. It is the translation into the language of the identification of the model of the differential equations of the motor which expresses a torque balance.

```

1 VelIdx = find(abs(velf) > max(abs(velf))/100);
2 TadIdx = [1:2,5]; % gravity and inertial terms
3 A = [ sin(posf/ntr*2*pi), cos(posf/ntr*2*pi),... % gravity
4       velf*2*pi,... % viscous friction
5       sign(velf),...% coulombian friction
6       accf*2*pi ]; % inertial torques
7 y = Kt*curf;
8 X_dyn = pinv(A(VelIdx, :))*y(VelIdx, :);
9
10 Tadd1 = abs(A(:,TadIdx)*X_dyn(TadIdx)).*sign(velf).*(sign(velf)>=0);
11 Tadd2 = abs(A(:,TadIdx)*X_dyn(TadIdx)).*sign(velf).*(sign(velf)<0);
12 A = [ A, Tadd1,Tadd2 ];
13 X_dyn = pinv(A(VelIdx, :))*y(VelIdx, :);

```

A small speed threshold is chosen (1/100 of the maximum speed). This is done because the friction, when the machine is stopped, changes its nature: it becomes a complex dynamic system. In the non-zero speed sections the model we are using works quite well.

Figure 3.11 shows the estimate of all torque components (on the left) and the estimate of friction motor torque (viscous and Coulumb) on the right.

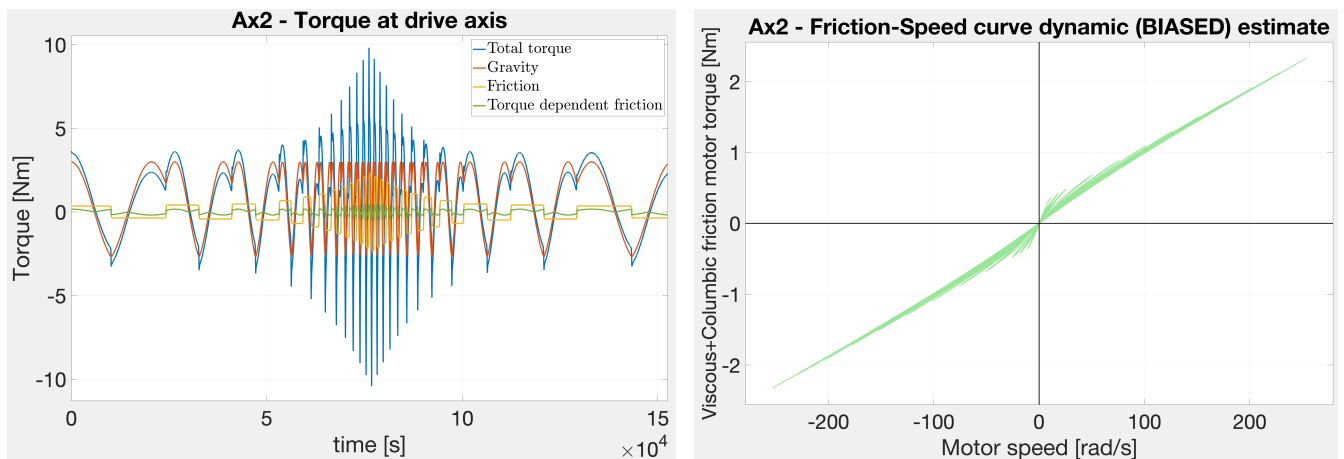


Figure 3.11. Estimate of all torque components (left) and the estimate of viscous and Coulumb friction motor torque (right)

Figure 3.12 shows the motor friction torque (viscous, Coulumb and torque dependent friction) as a

function of position for axis 2 with axis 3 extended (left) and for axis 3 (right).

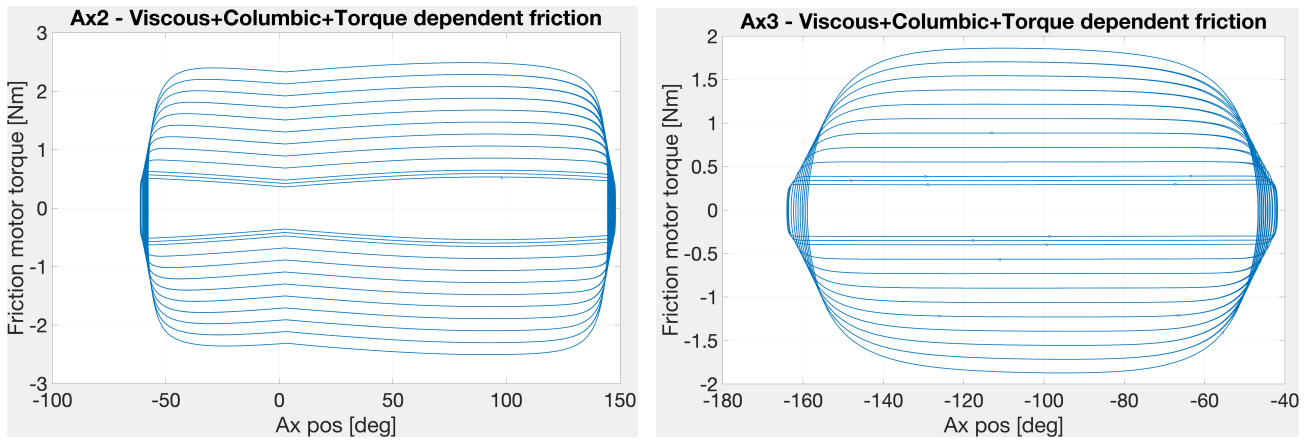


Figure 3.12. Motor friction torque (viscous, Coulumbic and torque dependent friction) as a function of position for axis 2 with axis 3 extended (left) and for axis 3 (right)

The plot on the left has a slightly tapered shape because it also takes into account the mesh friction which is a function of the acceleration. The plot of axis 3 seems more regular (we can see less of the effect of mesh friction).

Second method of estimation

In the second method, the estimated gravity is subtracted from the current. It is called detrending (the effect of gravity is removed). Figure 3.13 shows the current before and after gravity detrending.

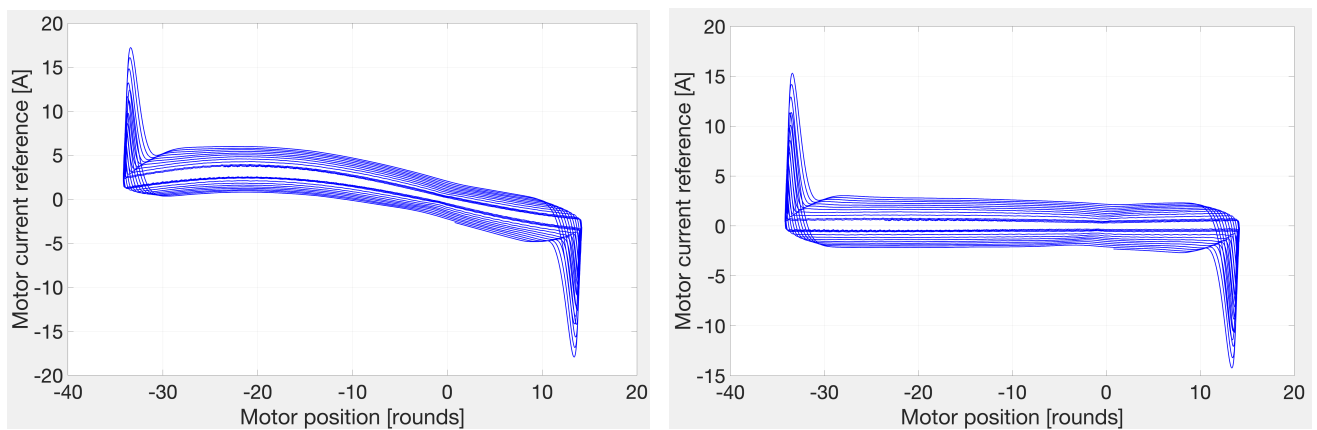


Figure 3.13. Current before (left) and after (right) gravity detrending

The fact that the current is constant at constant speed is an abstraction: the mesh friction makes the current at constant speed not perfectly constant, because it changes across the entire profile.

At the beginning and at the end there are the acceleration and deceleration phases, which correspond to the positive and negative current peaks: they are cut and the currents at constant speed are averaged.

The friction curve is constructed by points in which each section at constant speed is averaged to the current when the machine goes in one direction and when it goes in the other direction.

Figures 3.14 and 3.15 show the friction curves obtained from the 3 movement programs analyzed.

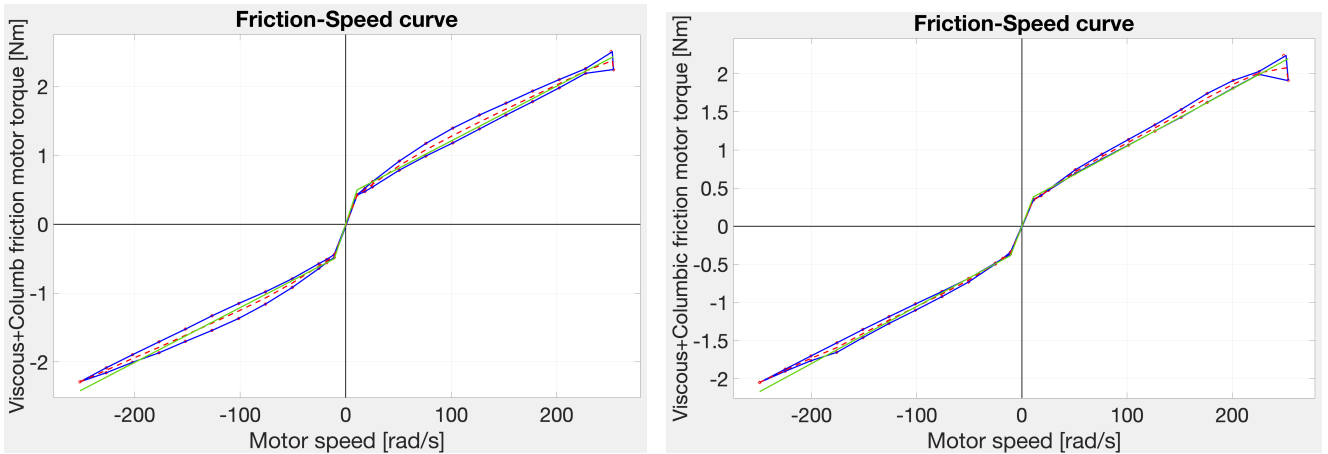


Figure 3.14. Friction curve of axis 2 with axis 3 extended (left) and with axis 3 folded (right)

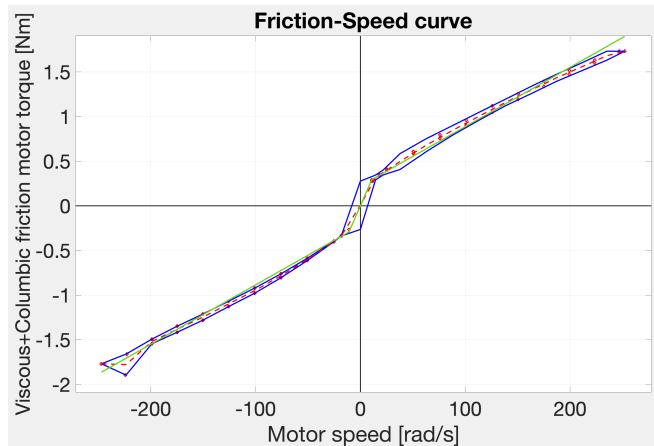


Figure 3.15. Friction curve of axis 3

The friction curve forms a hysteresis cycle. There are two curves because, depending on whether the section is traveled at decreasing or increasing speeds, different values are recorded: the system

has a memory effect, therefore it is something nonlinear. We approximate the average curve: we lose something at the level of detail but we have a usable simplification.

Calibration of friction values

Tables 3.1, 3.2, 3.3 show the reports of the friction values obtained from the two parameter estimation methods and the average of the tests, for axis 2 (with axis 3 extended and folded) and for axis 3.

| | Medium viscous friction [Nm/(rad/s)] | Dynamic dry friction [Nm] |
|----------|--------------------------------------|---------------------------|
| Method 1 | 0.0081085 | 0.27149 |
| Method 2 | 0.0079172 | 0.41535 |
| Average | 0.0080129 | 0.34342 |

Table 3.1. Friction parameters of axis 2 with axis 3 extended

| | Medium viscous friction [Nm/(rad/s)] | Dynamic dry friction [Nm] |
|----------|--------------------------------------|---------------------------|
| Method 1 | 0.007361 | 0.23871 |
| Method 2 | 0.0072773 | 0.31747 |
| Average | 0.0073192 | 0.27809 |

Table 3.2. Friction parameters of axis 2 with axis 3 folded

| | Medium viscous friction [Nm/(rad/s)] | Dynamic dry friction [Nm] |
|----------|--------------------------------------|---------------------------|
| Method 1 | 0.0065793 | 0.22582 |
| Method 2 | 0.0066119 | 0.22402 |
| Average | 0.0065956 | 0.22492 |

Table 3.3. Friction parameters of axis 3

We can see that axis 2 in a different condition has a slightly lower friction, but the order of magnitude does not change: this shows that friction is not a constant. The gearbox of axis 3 is a little smaller than that of axis 2, therefore it is reasonable that the level of both viscous and Coulomb friction is lower.

In conclusion, for both axis 2 and axis 3 I choose the average values of the tests, considering the other values as upper/lower limits.

3.9 Model identification of the Racer 7-1.10

The goal of this part is the minimum characterization of the Racer 7-1.0 (identification of a realistic model of axes 2 and 3). This identification is not the object of the thesis but is a support to highlight the difference between the models we use and reality. Identification is very important in the observer's project because the more precise is the model, the more reliable the reconstruction is.

A systematic campaign of identifications was carried out on axes 2 and 3 in poses in which the angle between the two axes varies. The control for identification is a PI with a position gain: it is a very simple control structure (it cannot be complicated because it would alter the test signal).

The results are of good quality (Figure 3.16 shows the various frequency response functions - complete and approximating - relating to the transfer function that links the reference current to the rotation speed of the motor of axis 2), and satisfy all the “traditional” validation criteria well:

- The complex conjugate poles alternate with complex conjugate transmission zeros (related to the two dominant frequencies of vibration)
- The minimum phase rotation does not exceed -180° and, asymptotically, tends to -90° .

The identified LTI models (modal Frf fit model) are used to create LTI observers that reconstruct the velocity of the arm of axis 2 (in the conditions in which the LTI model is reliable).

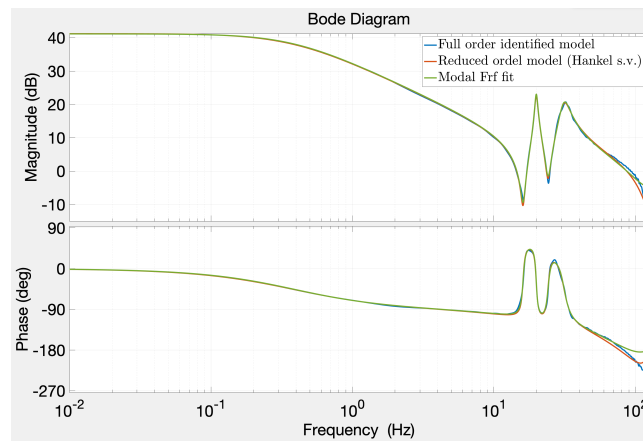


Figure 3.16. Identified LTI models of axis 2

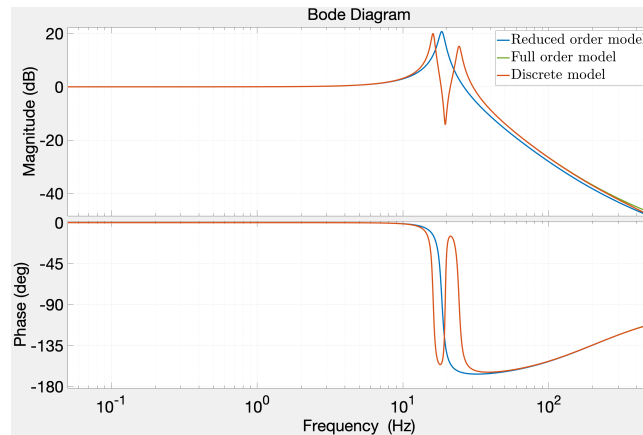


Figure 3.17. Transfer function obtained using the model of axis 2 only superimposed to that obtained with the complete model

Figure 3.17 shows the transfer function between motor speed and speed of the center of mass of

the arm using the reduced order model of axis 2 only and using the complete model obtained from the identification data together with its discrete equivalent.

We tend to attribute the interaction between axes 2 and 3 as if they were isolated (as if they were mounted on a perfectly rigid platform), but the response we see when identifying axis 2 is very influenced by the base. Therefore the structure acts as an additional part of the system.

If the movements of axis 2 are considered (with the other axes stationary), this “filter”, applied to the real speed of the axis 2 motor, provides a reliable reconstruction of the rotation speed of the link and can be used as a virtual sensor.

4. Simulation results

The simulation test is done in a context in which we have full control of the parameters as complexity. The chosen model is a reduced order system in which axis 2 is considered the observed system and axis 3 as additional dynamics. The plant is simulated as if it were a double pendulum in which the second link is kept braked but has an elastic element that activates it and therefore presents the typical effect of mutual inertial couples. Doing this, the coupling between axes 2 and 3 can be studied. When axis 3 is energized by the current of axis 2, the unbraked part of the dynamics of link 3 manifests itself in the form of vibrations that impact the dynamics of link 2.

It is important to highlight that an additional test signal modeled as white noise is used to energize the system and to verify its behavior (in reality it is not used).

Figure 4.1 shows the Simulink setup used for the simulation.

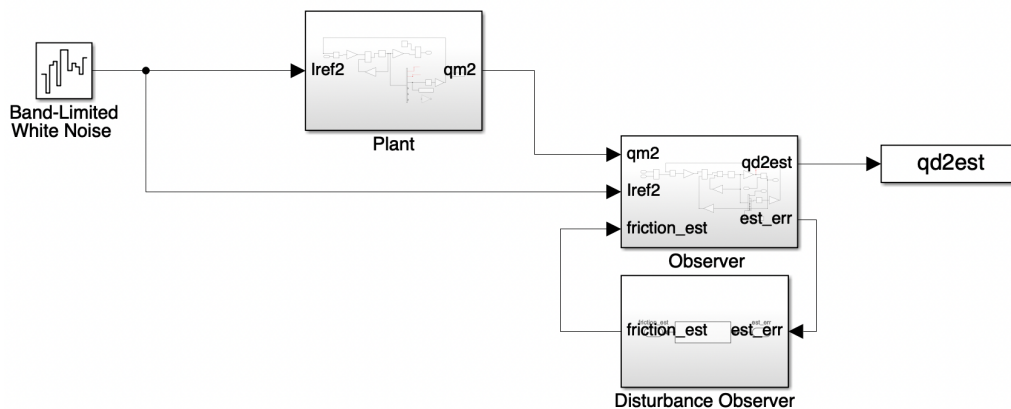


Figure 4.1. Simulation setup in Simulink

In the following sections, only the results of the 5-state and 6-state observers are shown because they are the most readable.

Pose of the manipulator

The reference pose of the manipulator for carrying out the experiments is chosen in such a way that the dynamics of axes 2 and 3 corresponds to that of a double pendulum.

The pose chosen for the simulations is (in degrees): $[0 \ 45 \ -110 \ 90 \ -90 \ -90]$.

Figure 4.2 shows the schematic representation of the chosen pose.

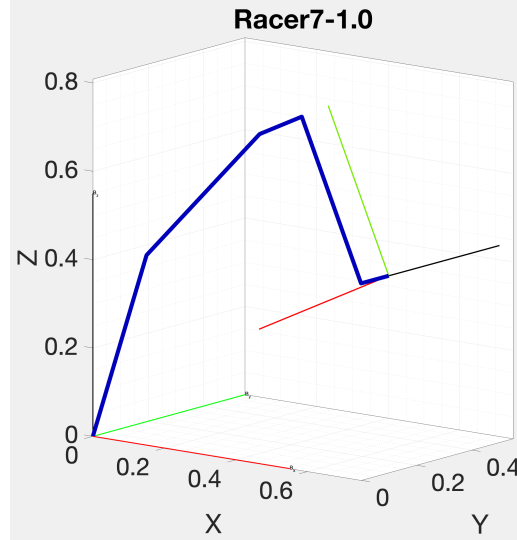


Figure 4.2. Representation of the pose chosen in simulation

The inertia matrix is reported in Figure 4.3.

Inertia matrix:

| | | | | | |
|---------|---------|---------|---------|---------|---------|
| 20.3791 | 0.0159 | 0.3356 | 0.2050 | -0.0734 | 0.0337 |
| 0.0159 | 14.3854 | 3.4358 | -0.2669 | 0.5350 | -0.2443 |
| 0.3356 | 3.4358 | 2.7927 | -0.4372 | 0.0656 | 0.0975 |
| 0.2050 | -0.2669 | -0.4372 | 0.4170 | 0.0000 | 0.0000 |
| -0.0734 | 0.5350 | 0.0656 | 0.0000 | 0.2025 | -0.0798 |
| 0.0337 | -0.2443 | 0.0975 | 0.0000 | -0.0798 | 0.2032 |

Figure 4.3. Inertia matrix

4.1 Compensation of disturbances

In the simulation there is no gravity, so it is as if it were perfectly compensated. There are only exogenous disturbances upstream of the speed and position states of the motor.

The friction disturbance is deterministic and its model coincides with the friction that appears in the plant. If friction compensation in feedforward is done, the disturbances would be completely canceled, so the effectiveness of the disturbance observer could not be evaluated. Therefore in simulation the two compensations are tested separately.

Disturbance observer analysis

Figure 4.4 shows the transfer function between the friction disturbance and the estimation error of the 5-state observer.

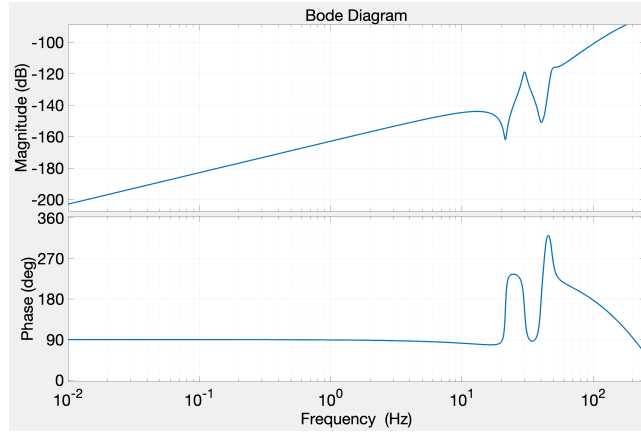


Figure 4.4. Transfer function between the friction disturbance and the estimation error of the 5-state observer

The additional state represents an additional torque input and provides an integrative action that generates a zero at the origin in the transfer function. The 5th state tends to absorb all the causes of error, but at the same time it does not allow to understand how the system work. This issue is the core of the so-called observability problem: with a 5th order observer it is not possible to physically distinguish what is mutual inertial torque acting on the center of mass from what is friction. In conclusion, the disturbance observer can only be designed on structures that do not have internal integral actions.

Figure 4.5 shows the transfer function between the friction disturbance and the estimation error of the 4-state observer.

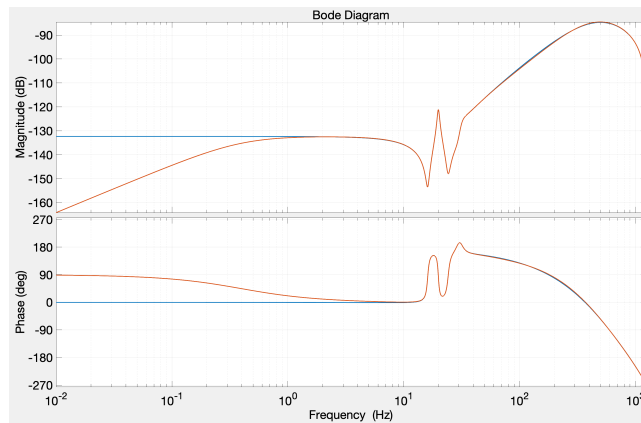


Figure 4.5. Transfer function between the friction disturbance and the estimation error of the 4-state Luenberger observer

There is no longer zero in the origin. The orange function represents the transfer function transformed by the addition of the regulator. These trends are the same as those of the 5th order observer. The addition of an external regulator to the observer, from the point of view of error reduction, achieves the same objective that the 5th state achieved: it tends to reduce the error to the minimum possible, but this time the integrative action is not inside the model of the system but is external. On a physical level, it describes the fact that a source of disturbance is acting on the system, independently of what we use as the model of the system. This is the correct way to handle friction.

Figure 4.6 shows the transfer function between the friction disturbance and the estimation error of the 6-state Luenberger observer and Kalman filter.

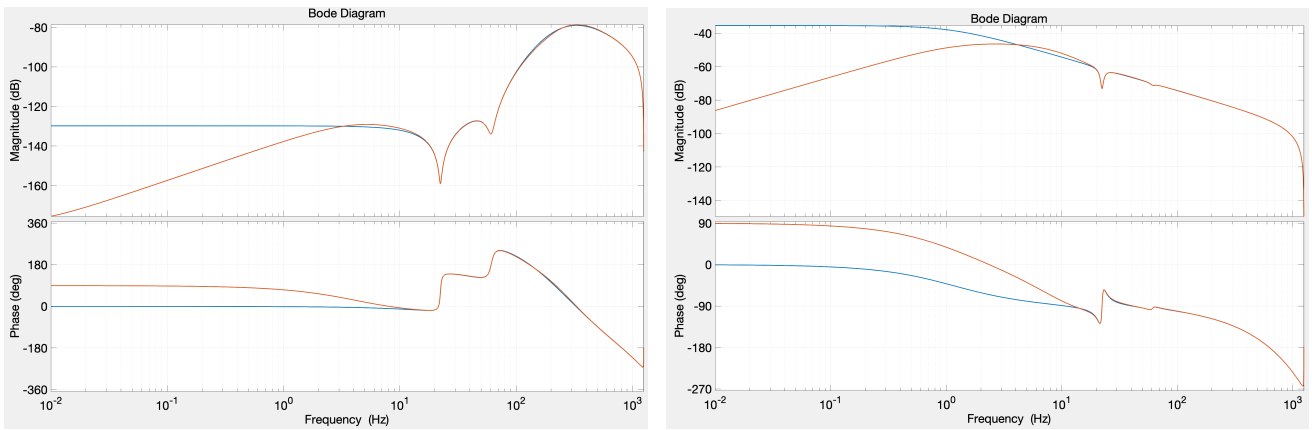


Figure 4.6. Transfer function between the friction disturbance and the estimation error of the 6-state Luenberger observer (left) and Kalman filter (right)

The transfer function obtained with the Luenberger observer is a typical response when there is no equivalent of the 5th state in the model. It tends to have a low gain but non-zero and a high frequency emphasis. In the transfer function with the Kalman filter the two poles corresponding to the vibration modes of the structure have almost disappeared. This means that the attenuation of the error on the motor position is stronger with the Luenberger observer.

As far as the 7-state observer model is concerned, simple techniques for tuning the Disturbance observer did not give good results, therefore the tuning of the Disturbance observer was not done.

Motor position

Figure 4.7 shows the motor position of axis 2 and its reconstruction.

With all types of observers, there are no visible differences on the motor position (which is the measured variable), because it is a state of the model that is most directly linked to the measurements (the observer works primarily to ensure that this state converges to its reference value). All model errors, missing parts, disturbances acting on the model that are not on the observer, create anomalous signals on the deep states (i.e., the part of the model's state vector which does not directly influence the measurements).

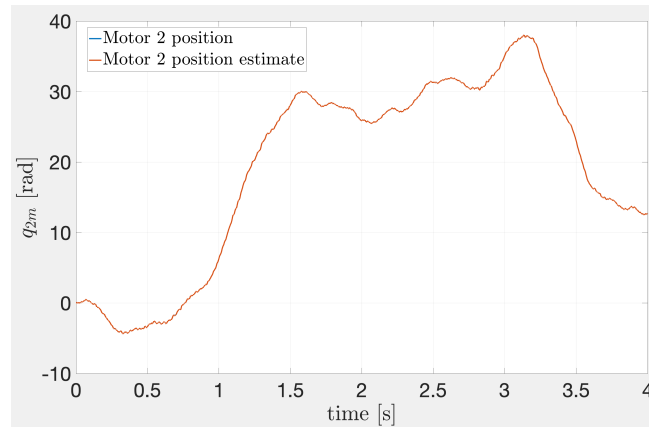


Figure 4.7. Motor position of axis 2 and its reconstruction

4.2 5-state Luenberger observer

The pole frequencies with which the best results are obtained, for a compromise between the presence of noise and minimization of the reconstruction error, are $2\pi \cdot [200, 300, 1000]$ rad/s with a damping $\zeta = 0.9$ (well damped poles).

Figure 4.8 shows the reconstruction of the state (speed of link 2) and the zoom into an area.

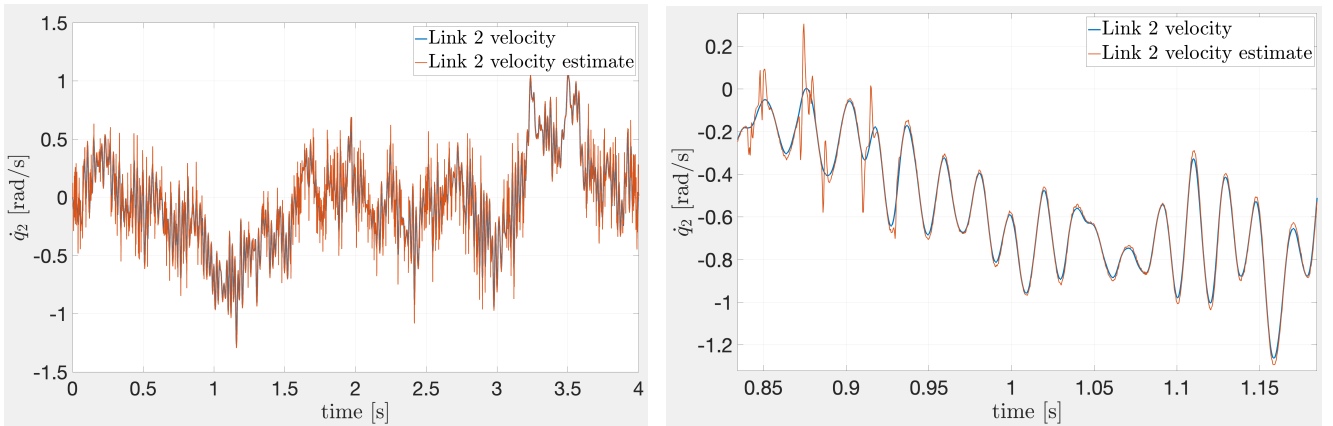


Figure 4.8. Reconstruction of the state with a 5-state Luenberger observer and relative zoom (right)

From Figure 4.9 which represents the reconstruction error and the friction of the plant, we can clearly see that there are peaks where there is a state transition of friction when passing from a situation where the axis is blocked by the static friction to a condition where the axis begins to slip.

To study how the observer manages to reconstruct the mutual inertial term, the τ_{ext} plot is superimposed to the acceleration of link 3 (deriving the speed of link 3) multiplied by the term (2,3) of the

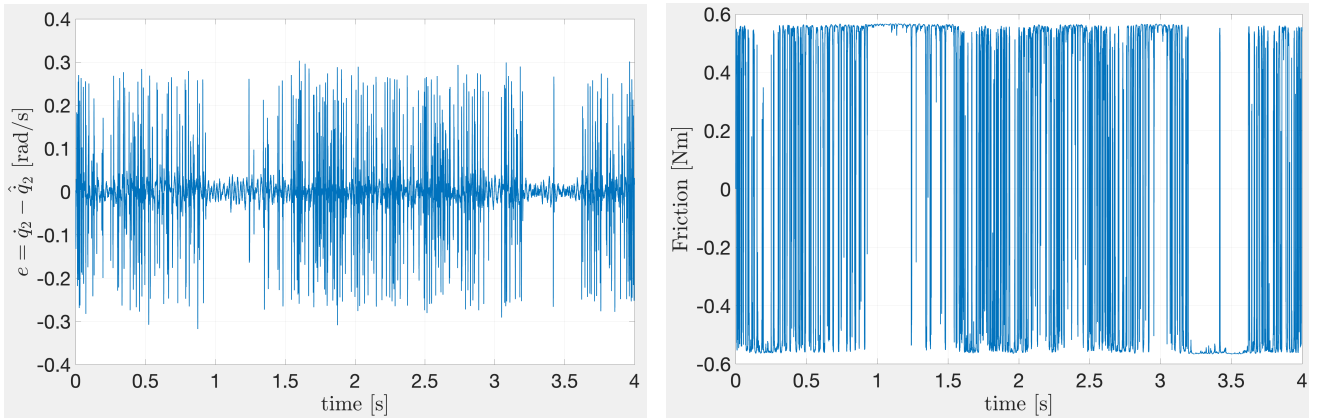


Figure 4.9. Reconstruction error (left) and friction of the plant (right)

inertia matrix. Figure 4.10 shows the result and the zoom into an area.

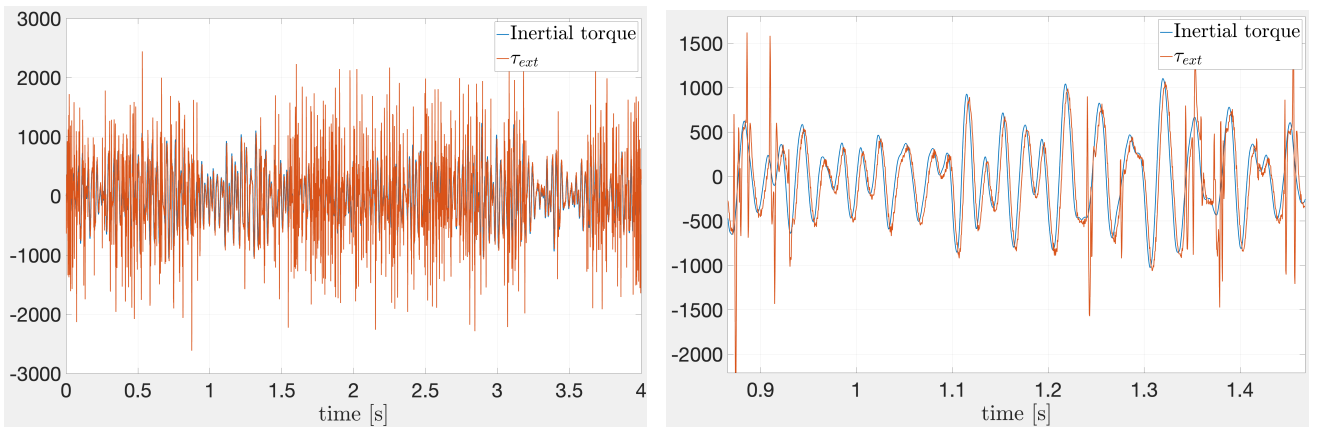


Figure 4.10. Mutual inertial term superimposed to the additional state and relative zoom (right)

The observer, who is not updated on the presence of friction, interprets it as an oscillation on the mutual inertial couple. Furthermore, we can see from the zoom that the observer reconstructs with a little delay.

In conclusion, if the observer is not informed of friction, the reconstruction of the state is wrong from the point of view of physical meaning (it contains fictitious trends).

Figure 4.11 shows the reconstruction of the state (speed of link 2) and of the mutual inertial torque adding friction compensation with the arctangent in the observer. We can see that the reconstructions are much better than before (there are no longer any peaks that were due to friction). In this way, it is demonstrated that the implementation of the observer is correct because the 5th state mimics the

interaction between axes 2 and 3 which is represented in plant but not in the observer model. The problem is that having a predictive model of friction that works well is not easy due to the variability of friction.

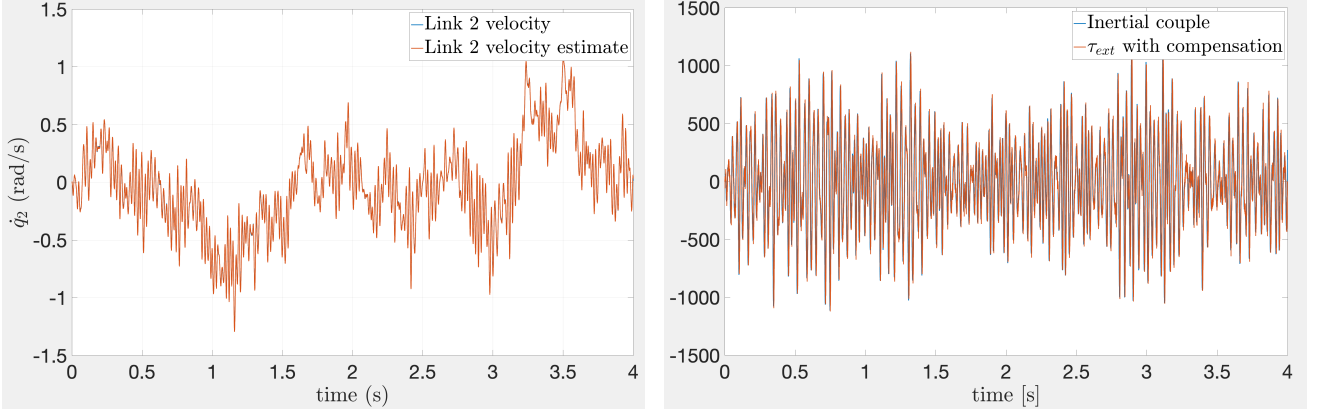


Figure 4.11. Reconstruction of the state with a 5-state Luenberger observer with friction compensation (left) and mutual inertial term superimposed to the additional state (right)

4.3 5-state Kalman filter

The obtained results with the 5-state Kalman filter are similar to those with the 5-state Luenberger observer. However, it is important to consider the covariance matrices chosen to achieve these results.

Matrix R is chosen as the standard deviation of the measured values from the real values obtained from measurements on a real machine.

$$R = 1.1039^{-6} \quad (4.1)$$

Matrix Q is chosen as a positive symmetric matrix of the type $Q = G \cdot G^T$. It is obtained with trial-and-error techniques.

$$G = \begin{bmatrix} 0.1 & \frac{1}{Ntr(2,2)} & 0.1 & 0 & 0 \\ \frac{1}{Ntr(2,2)} & 0.1 & \frac{1}{Ntr(2,2)} & 0.1 & 0 \\ 0.1 & \frac{1}{Ntr(2,2)} & 0.1 & \frac{1}{Ntr(2,2)} & 0 \\ 0 & 0.1 & \frac{1}{Ntr(2,2)} & 0.1 & 0 \\ 0 & 0 & 0 & 0 & 500 \end{bmatrix} \quad (4.2)$$

As it can be seen, the biggest diagonal value has been assigned to the element representing the additional state which is the most uncertain state of the system. Off-diagonal values represent interactions between different states: e.g., the position of the joint and the position of the motor are related by the transmission ratio.

A similar criterion is used for the choice of the Q matrix for the 7-state Kalman filter.

$$G = \begin{bmatrix} 0.01 & \frac{1}{Ntr(2,2)} & 0.1 & 0 & 0 & 0 & 0 \\ \frac{1}{Ntr(2,2)} & 1 & \frac{1}{Ntr(2,2)} & 0.1 & 0 & 0 & 0 \\ 0.1 & \frac{1}{Ntr(2,2)} & 0.01 & \frac{1}{Ntr(2,2)} & 0 & 0 & 0 \\ 0 & 0.1 & \frac{1}{Ntr(2,2)} & 500 & 0 & 0 & 0 \\ 0 & 0 & 0 & 0 & 5 \cdot 10^6 & 100 & 0 \\ 0 & 0 & 0 & 0 & 100 & 1 & 0 \\ 0 & 0 & 0 & 0 & 0 & 0 & 1 \end{bmatrix} \quad (4.3)$$

Also in this case, the biggest diagonal value has been assigned to the element representing the additional state that is the most uncertain state of the system.

4.4 6-state Luenberger observer

In this case, to achieve the results obtained with the previous observers, the pole frequencies can be lowered to $2\pi \cdot [40, 80, 100]$ rad/s, with a damping $\zeta = 0.9$. Even with lower eigenvalue frequencies (therefore with a more filtering control action), the states can be reconstructed very well because the 6th order observer has already internally represented the dynamic interaction between the axes.

Figure 4.12 shows the reconstruction of the state (velocity of link 2) with the 6-state Luenberger observer (with Disturbance observer) and the zoom into an area.

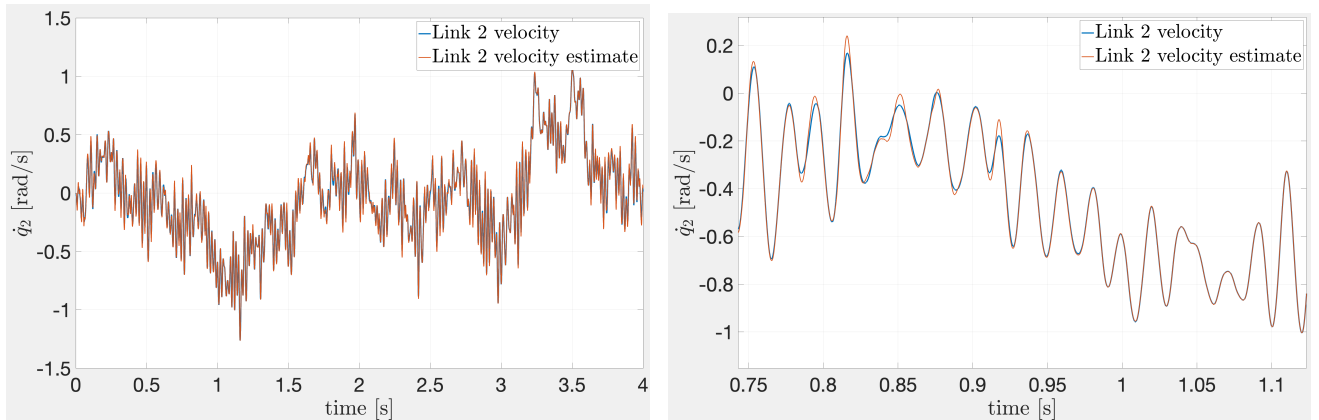


Figure 4.12. Reconstruction of the state with a 6-state Luenberger observer (left) and relative zoom (right)

State reconstruction is very good in this case. As it can be seen from Figure 4.13, the error is reduced by an order of magnitude compared to the 5-state observer (10^{-2} instead of 10^{-1}).

This is partially due to the action of the disturbance observer. Figure 4.14 shows the simulated friction of the plant superimposed on the disturbance observer estimate.

When friction maintains the state for a long time the estimate tends to be very good, instead when friction often changes state the external ring acts as a sort of filter, because the transition is very fast

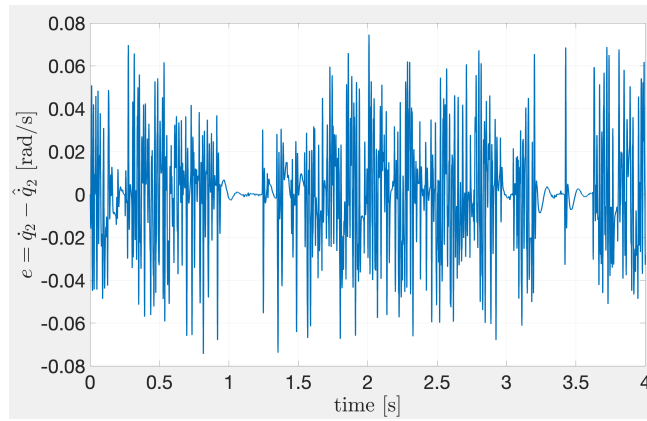


Figure 4.13. Reconstruction error of the 6-state Luenberger observer with Disturbance observer

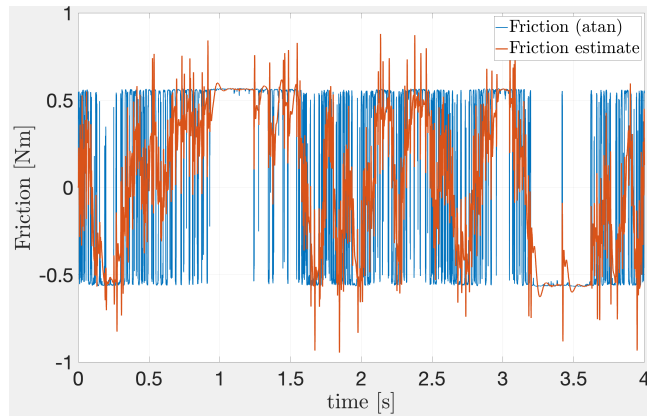


Figure 4.14. Friction estimate of the disturbance observer and simulated friction

but the regulation system has a dominant pole at 10 Hz (it cannot follow frequencies and dynamics faster than 10 Hz).

This is fundamental to understand the importance in reconstructing the state of modeling well all the disturbances that act on the system: observers work well only if all the cause-and-effect relationships are known and represented. When friction is represented well, the reconstruction of the state is perfect.

4.5 6-state Kalman filter

Matrix R is chosen as discussed in Section 4.3. Matrix Q is chosen as a positive symmetric matrix of the type $Q = G \cdot G^T$. It is obtained with trial-and-error techniques.

$$G = \begin{bmatrix} 0.1 & 0 & \frac{0.1}{Ntr(2,2)} & 0.01 & 0 & 0 \\ 0 & 0.1 & 0 & 0 & 0.01 & 0 \\ \frac{0.1}{Ntr(2,2)} & 0 & 100 & \frac{0.1}{Ntr(2,2)} & 0 & 0.1 \\ 0.01 & 0 & \frac{0.1}{Ntr(2,2)} & 0.1 & 0 & \frac{0.1}{Ntr(2,2)} \\ 0 & 0.01 & 0 & 0 & 0.1 & 0 \\ 0 & 0 & 0.1 & \frac{0.1}{Ntr(2,2)} & 0 & 100 \end{bmatrix} \quad (4.4)$$

As it can be seen, the biggest diagonal value has been assigned to the element representing the position and velocity of motor 2, i.e., the measurable states.

Figure 4.15 shows the reconstruction of the state (velocity of link 2) with the 6-state Kalman filter (with Disturbance observer) and the corresponding reconstruction error.

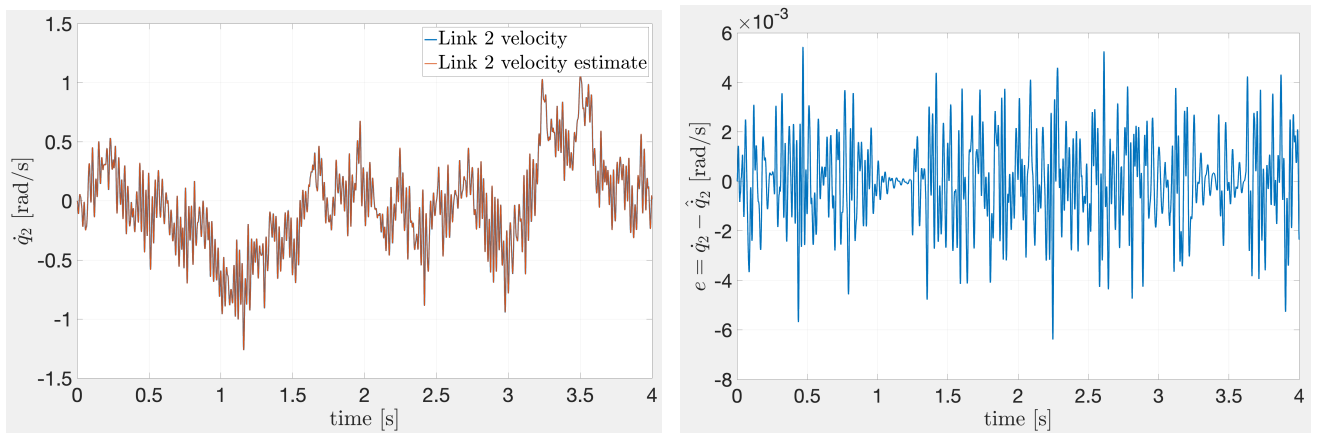


Figure 4.15. Reconstruction of the state with a 6-state Kalman filter (left) and reconstruction error (right)

The two curves are almost superimposed, in fact the maximum error is of the order of 10^{-3} , therefore it is the best result achieved for the simulation tests.

4.6 4-state Luenberger observer

In the case of the 4-state Luenberger observer, the pole frequencies are raised to $2\pi \cdot [500, 600]$ rad/s, with a damping $\zeta = 0.9$. This is very important to highlight because in a model that contains a partial dynamic with no additional state to compensate for the missing part of the true dynamics, the correction action must be more stringent (the gains must be higher) to achieve the same results.

5. Experimental results

This chapter shows the achieved results by testing the observers on real data. First, a virtual sensor obtained from the identification of the manipulator model is used and then the final test is done with the real gyroscope. The difference between the virtual sensor and the real gyroscope is that the real gyroscope always measures speeds (I may not even have a model of the dynamics of interest), whereas the virtual sensor is reliable in the specific condition in which the identified model is valid. In addition, the virtual sensor provides an estimate based on a linear model, while the real gyroscope does not make any prediction based on a mathematical model. In the situation in which the axis is stopping, there is an important non-linearity given by the entry into static friction regime, which tends to dampen the vibrations a lot, so the linear model could give a wrong representation.

Movement program

A motion recording of axis 2 is taken by assigning a relative pose with axis 3 held braked (there is a 90° angle between axis 2 and 3). The program moves axis 2 back and forth (not between the same two positions but also putting intermediate positions) at different speeds, with time intervals in which axis 2 remains still for a few seconds (because in real industrial applications it happens that one or more axes are kept stationary).

The matrices should be recalculated every 10 ms, because the inertia matrix $M(q)$ is a variable matrix and varies as the position of the robot varies. However, given the complexity of the problem, the experimentation is done in conditions in which we only move axis 2 and keep axis 3 and the other axes stationary in a certain condition. The working condition of the manipulator varies because axis 2 moves, but for the purposes of the reduced model it does not change, because the inertias of axes 2 and 3 remain the same. The model representing axes 2 and 3 can therefore be calculated only in one condition.

Pose of the manipulator

The initial pose of the manipulator is chosen in such a way that the dynamics of axes 2 and 3 corresponds to that of a double pendulum.

The initial pose of the manipulator is (in degrees): $[0, 87, -42, 90, 0, 90]$

Figure 5.1 shows the schematic representation of the chosen pose.

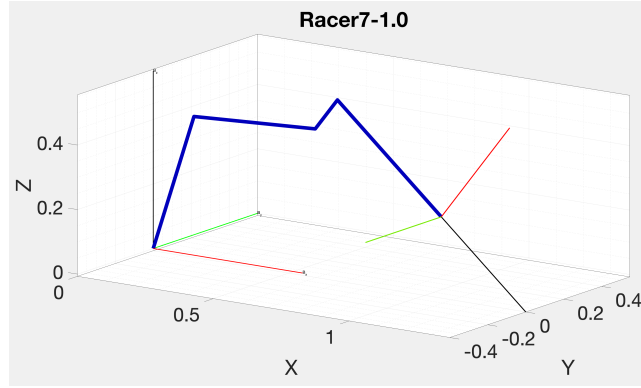


Figure 5.1. Representation of the initial pose chosen in simulation

5.1 Models comparison

5.1.1 Fit percentage

The goal of this thesis is to make a quality reconstruction of certain signals, so it is better to introduce a metric that measures it. There is a criterion called fit percentage which, given two signals, measures the similarity of the signals on average, according to the following equation:

$$FIT = 100 \cdot \left(1 - \frac{\|Y - \hat{Y}\|}{\|Y - \bar{Y}\|} \right) \quad (5.1)$$

where Y is the reference signal, \hat{Y} is the signal reconstruction, \bar{Y} is the mean of the reference signal.

5.1.2 Nominal and identified data

Observers work well if the model is well aligned with reality. This is especially true if there is a single sensor on the motor position. If there were other sensors (i.e., more information about the states), it would be easier to accept qualitative modeling. We test the observer with two models:

1. A first approximation model (nominal, i.e., with data obtained from mechanical design), which is not very precise.
2. An identified model, which is local and optimized on the machine in a certain condition.

Everything that diverges from reality becomes a disturbance and creates artifacts on the estimate of the state. For this reason, it is important to analyze the difference in the reconstruction of the state between a nominal model and a model that better represents reality.

5.2 Gravity and friction compensation

Gravity compensation is done as explained in Section 3.4. Correctly locating gravity as a torque acting on the center of mass of the arm is important to have a plausible reconstruction of the state.

Figure 5.2 shows the output of the disturbance observer without gravity compensation overlapped with the calculated gravity.

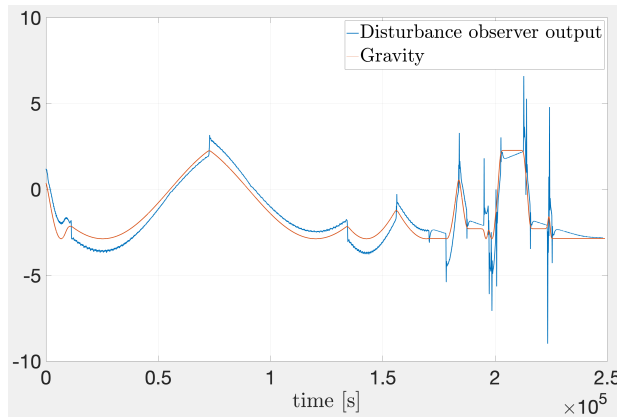


Figure 5.2. Disturbance observer output without gravity compensation overlapped with gravity estimate

The gravity waveform appears in the external observer. It is a pseudo-periodic signal, whose frequency varies with the rotation speed (the period gets shorter as the speed increases).

Figure 5.3 shows the output of the disturbance observer with gravity compensation.

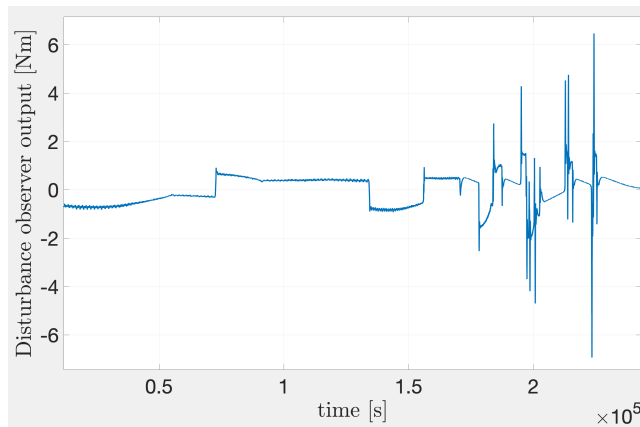


Figure 5.3. Disturbance observer output with gravity compensation

In reality, the arctangent model does not include all the friction components: there are the sliding friction of the gear teeth which varies as a function of the pressure of the transmitted torque, and some friction components at low speed (static friction) which are not estimated by the arctangent model.

For this reason, both feedforward compensation and disturbance observer are used in these tests because they have two different goals.

Normally in real systems the presence of the disturbance observer reduces the velocity reconstruction anomalies that appear when friction changes state. For example, if the motor is stopped and then starts rapidly with a positive acceleration but there is static friction, if it is not separated from the driving torque, in the first 20 or 30 ms of the movement the speed estimate of the reconstructed axis changes sign (it presents a non-physical trend). Therefore the contribution of the disturbance observer is above all in the transition from a condition of static friction to a condition of dynamic friction.

Figure 5.4 shows a portion of the link 2 velocity reconstruction with the 6-state Luenberger observer with and without Disturbance observer.

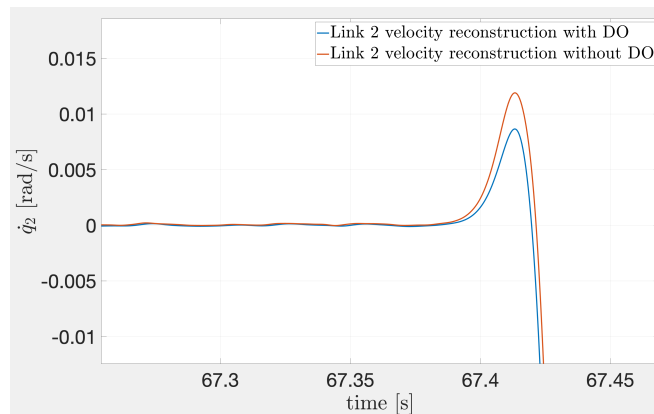


Figure 5.4. Link 2 velocity reconstruction with the 6-state Luenberger observer with and without Disturbance observer

In the reconstructions with disturbance observer, a spike in the opposite direction is still seen even if of reduced amplitude. This means that there are disturbing torques (some component of friction or some non-linearity of the transmission) not correctly modeled, which are interpreted as state variations on the model even if they are not.

When we insert the noise, the problem is less visible because, being a package of persistent sinusoids, they make the motor move continuously, preventing it from entering the static friction regime.

5.3 Motor torque disturbance compensation

In the tests with the real gyroscope motor torque oscillations are compensated [20]. The torque ripple in permanent magnet brushless motors appears as an irregularity in the generation of the torque, which shows a ripple added to the nominal torque provided by motor. They are oscillations that are not related to oscillating transients of the mechanical structure, but are linked to the motor. Their frequency is inversely proportional to the rotation speed and directly proportional to the current. They can be seen in precise operations, for example sealing and arc welding, because they occur at low speed.

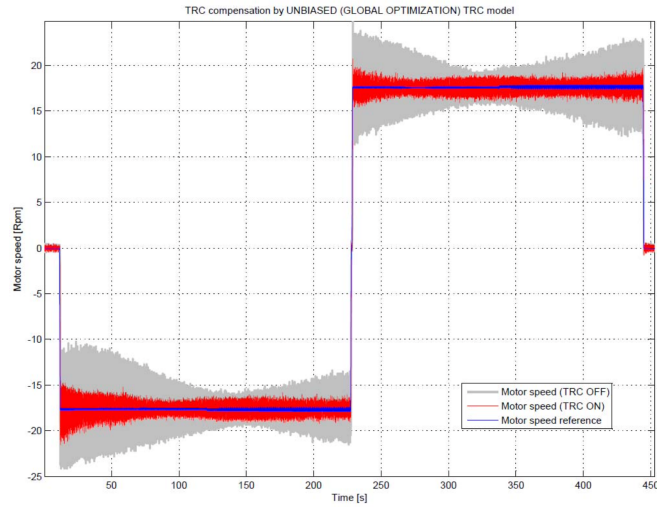


Figure 5.5. Torque ripple compensation effect [20]

A calibration of the drives of axes 2 and 3 was made so that the torque disturbances of the motors are minimized in amplitude (as shown in Figure 5.5).

5.4 Torque-current relationship

To increase the model's fidelity compared to reality, the effects of motor saturation in the current-torque relationship are also taken into account. In reality, the relationship between current and torque is a non-linear function of the current and the rotation speed of the motor: as the current increases, the value of K_t decreases linearly with the current (as shown in Figure 5.6).

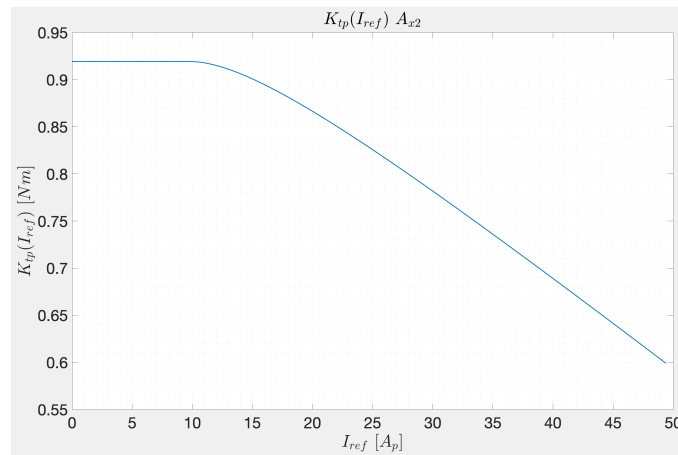


Figure 5.6. Saturation of the magnetic flux in the air gap

This effect is called saturation of the magnetic flux in the air gap and causes apparent torque loss effects. In the air gap there are also, significantly, the flux lines of the magnetic induction caused by the stator currents. The stator magnetic induction adds to the rotor magnetic induction, reducing the total magnetic induction and also the total magnetic flux useful for generating the torque. Therefore, for the same amount of generated torque, much more current is needed. This reduces the maximum amplitude of the counter electromotive force voltages that determines a proportional reduction in the produced mechanical torque.

On the considered motor the relationship is fine up to around 15 Ampere.

In this case, current preprocessing is used to correct distortions introduced by saturation. It means imposing a linearized trend on the input currents to the regulator (the extreme peaks of current are compressed). It's like applying an equalizer to the current signal.

5.5 Virtual sensor

Having a good identification of the dynamic response (as discussed in Section 3.9) not only gives a good identification of the transfer function between the current and the velocity of link 2, but also gives a functional relationship between the rotation speed of the motor and the velocity of the link. This transfer function is a virtual sensor, allowing to make a reasonable prediction of the way the arm works when the motor has a specific trend.

Figure 5.7 shows the link 2 velocity reconstruction superimposed to the virtual sensor. The first part of the signal reconstruction has been cut to avoid the transient.

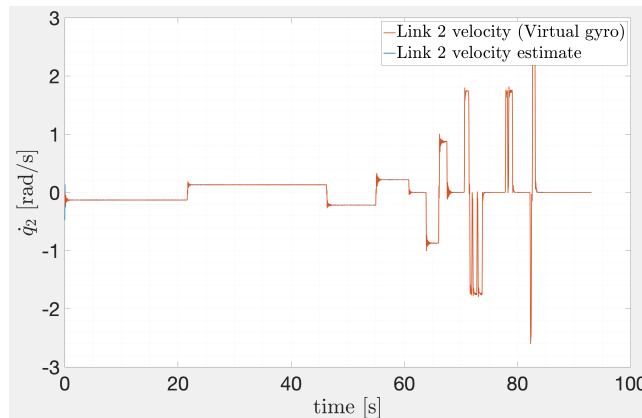


Figure 5.7. Link 2 velocity reconstruction superimposed to virtual sensor

In the following, details of the speed reconstructions of link 2 are shown. In one detail there is a reversal of motion, while in another (the one with 3 peaks) there are quite rapid stops and starts (the machine never stops).

Figure 5.8 shows two details of the velocity reconstruction of link 2 with the 6-state Luenberger observer. The pole frequencies are set to $2\pi \cdot [200,250,300]$ rad/s with a damping $\zeta = 0.9$.

The frequencies of the poles are different from those chosen in simulation (Section 4.4). All the various types of tested observers show the same result. The only one that shows a different result is the

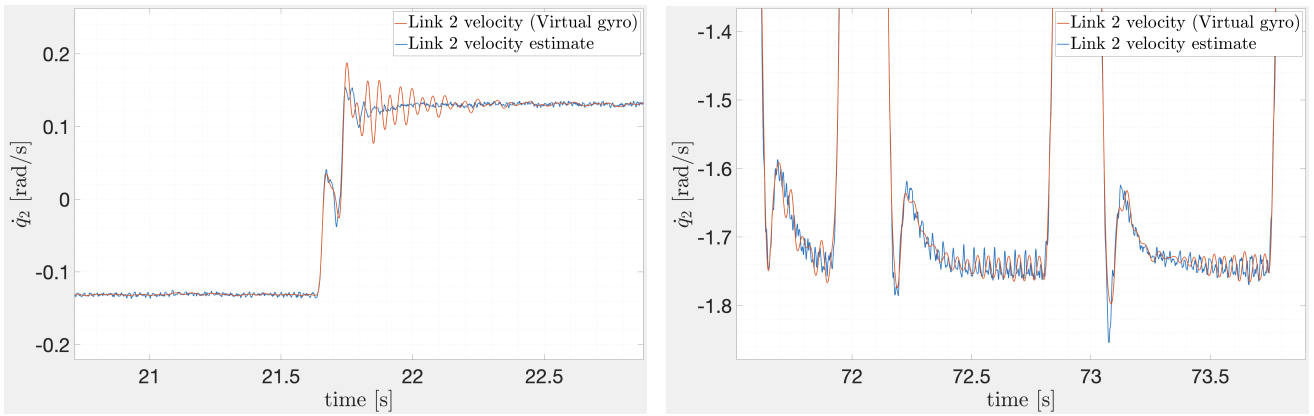


Figure 5.8. Link 2 velocity reconstruction using 6-state Luenberger observer with identified data and virtual sensor (zoom)

6-state Kalman filter.

Figure 5.9 shows two details of the velocity reconstruction of link 2 with the 6-state Kalman filter. The covariance matrices Q and R are set as discussed in Section 4.5.

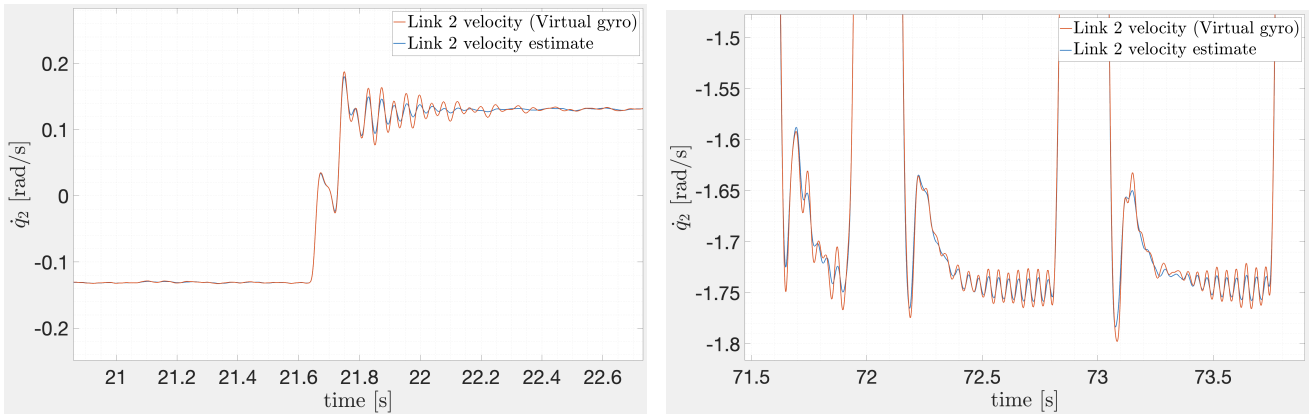


Figure 5.9. Link 2 velocity reconstruction using 6-state Kalman filter with identified data and virtual sensor (zoom)

On real data the observers have a different oscillating transient but the one that works best is the 6-state Kalman filter, comparing it with the virtual sensor. The prediction of oscillatory motion that the identification-based predictor gives does not appear in the result of the other observers.

The reason is the following: since it has very low gains compared to the other observers, the 6-state Kalman filter is working too much in prediction and not enough in correction (since it has a predictive model that predicts oscillations, it keeps them in the estimate).

5.5.1 Final results with virtual sensor

Tables 5.1 and 5.2 show the fit percentages obtained with all types of observers compared to the virtual sensor.

| N. states | Kalman filter | | |
|-----------|----------------------|----------------|-----------------|
| | Disturbance observer | Nominal data | Identified data |
| 6-state | YES | 97.1765 | 98.7898 |
| 5-state | NO | 97.7940 | 97.4430 |
| 7-state | NO | 97.8229 | 97.5854 |

Table 5.1. Kalman filter results on real data (virtual sensor)

| N. states | Luenberger observer | | |
|-----------|----------------------|----------------|-----------------|
| | Disturbance observer | Nominal data | Identified data |
| 6-state | YES | 97.8447 | 97.7528 |
| 5-state | NO | 97.7984 | 97.5821 |
| 4-state | YES | 97.8949 | 97.7040 |

Table 5.2. Luenberger observer results on real data (virtual sensor)

The fit percentages are approximately the same for all types of observers. As mentioned before, the model that performs best when compared to the virtual sensor is the 6-state Kalman filter, reaching a fit percentage of 98.7898% using the identified data for the model.

5.6 Gyroscope

In the final experiments the observers are validated using a Xsens gyroscope. This device contains gyroscopes and accelerometers and can be used to measure vibrations in the form of a linear acceleration signal and rotation speed of the link on which it is located.

We place the gyroscope directly above axis 2 (as shown in Figure 5.10) and we record the gyroscope signal and synchronize it in time with the machine’s acquisition by interpolating it at 400 μs . We take the second channel into consideration because it is the one closest to the working axis (axis y of the sensor is approximately parallel to the axis of rotation of the link).

Acquisitions were made at 400 Hz and 1600 Hz. Then a program with more exciting characteristics was tested.

5.6.1 Trajectory at 400 Hz

Figure 5.11 shows the link 2 velocity reconstruction superimposed to the real gyroscope with the 400 Hz trajectory. The first part of the signal reconstruction has been cut to avoid the transient.

In the following, details of the speed reconstructions of link 2 are shown. In one detail there is a reversal of motion, while in another (the one with 3 peaks) there are quite rapid stops and starts.

Figure 5.12 shows two details of the velocity reconstruction of link 2 with the 6-state Luenberger observer, with the poles frequency set as discussed in Section 5.5.



Figure 5.10. Xsens gyroscope above axis 2 of the manipulator

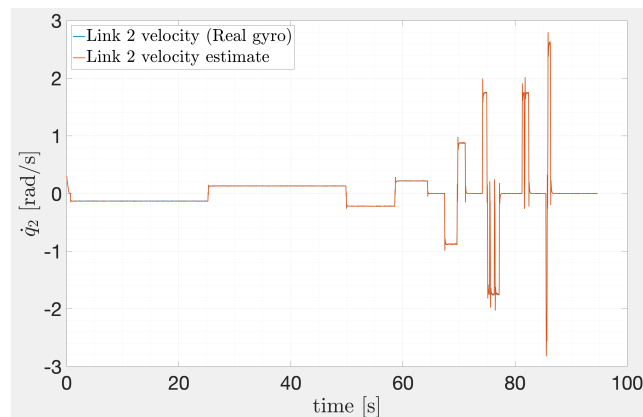


Figure 5.11. Link 2 velocity reconstruction superimposed to real gyroscope (400 Hz trajectory)

Figure 5.13 shows two details of the velocity reconstruction of link 2 with the 6-state Kalman filter. The covariance matrices Q and R are set as discussed in Section 4.5.

The 6-state Kalman filter tends to initially trigger oscillations that the real gyroscope does not let us see (afterwards it settles down correctly). This means that its correction ability is slow.

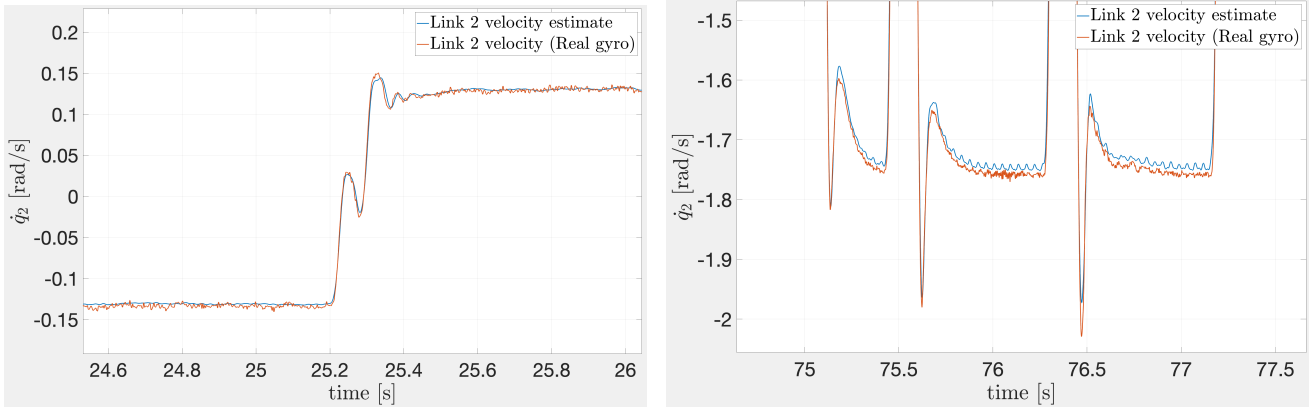


Figure 5.12. Link 2 velocity reconstruction using 6-state Luenberger observer with identified data and real gyroscope (zoom)

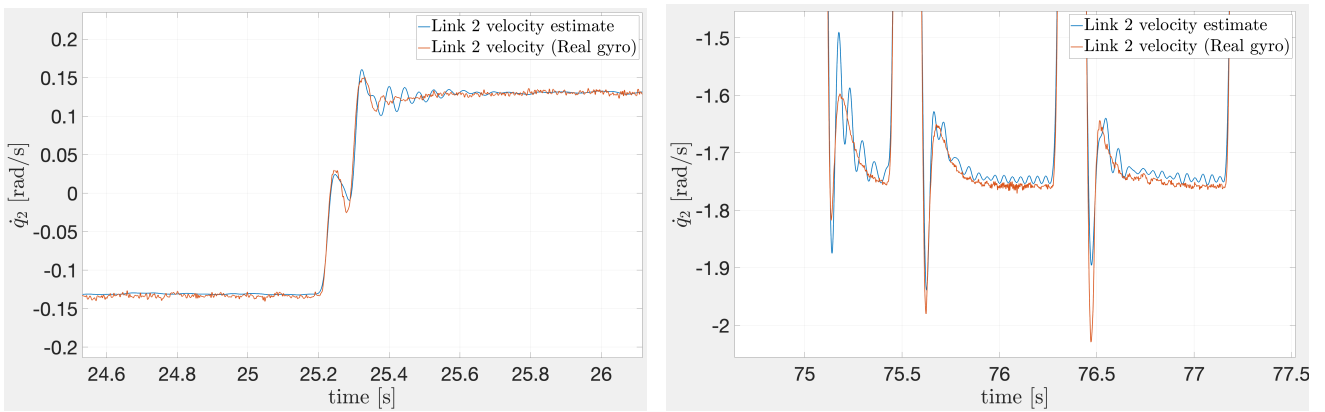


Figure 5.13. Link 2 velocity reconstruction using 6-state Kalman filter with identified data and real gyroscope (zoom)

The important thing that can be seen is that the virtual gyroscope showed more evident oscillations than in the real gyroscope. The reasons may be the following:

- The virtual gyroscope model is linear and the effects of friction may dampen the vibrations a lot. The nonlinear friction on the gearbox appears to have strong damping capacity.
- There is also a problem of energization: if normal functioning signals are used, the energy level is not such as to create persistent oscillations and the friction present in the transmissions is probably enough to dampen the signal.

The Hephestos project in [21] presents an analogy with the obtained result. The result of a simulation on a machining path is shown in Figure 5.14. This example is important because it compares the

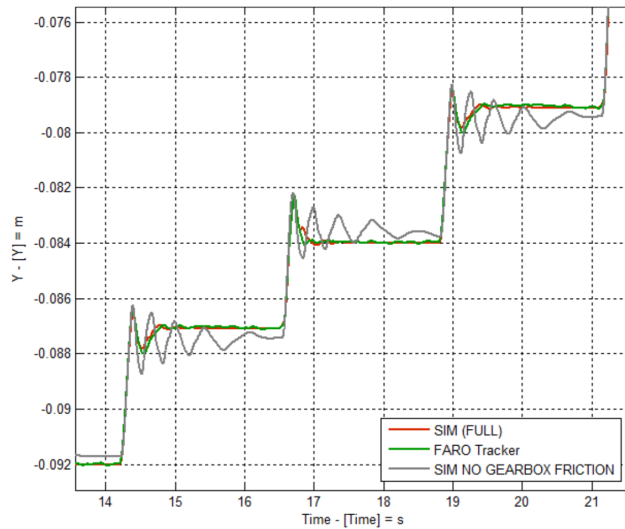


Figure 5.14. Hephestos project simulation [21]

simulation (red) with real machine data taken with the laser tracker (green). In a second simulation (grey) the Coulomb friction acting on axis 1 had been removed: what looked like an overshoot became a triangular oscillation (i.e., a non-linearity effect). In reality and in a realistic simulation it cannot be seen, because the amount of non-linear friction on the gearbox output is enough to absorb the vibration.

Even in the considered case, the linear model predicts an under-damped behavior which does not exist in reality, because there are non-linearities or frictions that dampen the output dynamics.

A test was also done with sampling at 1600 Hz to see if richer information emerged by increasing the sampling frequency of the gyroscope compared to sampling at 400 Hz. However, the data confirms the fact that there is no oscillation that we lose because of the instrument. Furthermore, these data are not used because 1600 Hz signals can have a sampling irregularity problem: there is no longer synchronous sampling.

To increase the ability of the 6-state Kalman filter to correct the information, the gains must be increased. The covariance matrices Q and R are changed as follows. Matrix R is chosen as discussed in Section 4.3. Matrix Q is chosen as a positive symmetric matrix of the type $Q = G \cdot G^T$. It is obtained with trial-and-error techniques.

$$G = \begin{bmatrix} 1 & 0 & \frac{0.1}{Ntr(2,2)} & 0.01 & 0 & 0 \\ 0 & 100 & 0 & 0 & 0.01 & 0 \\ \frac{0.1}{Ntr(2,2)} & 0 & 1 & \frac{0.1}{Ntr(2,2)} & 0 & 0.1 \\ 0.01 & 0 & \frac{0.1}{Ntr(2,2)} & 1 & 0 & \frac{0.1}{Ntr(2,2)} \\ 0 & 0.01 & 0 & 0 & 1 & 0 \\ 0 & 0 & 0.1 & \frac{0.1}{Ntr(2,2)} & 0 & 1 \end{bmatrix} \quad (5.2)$$

As it can be seen, the uncertainty raises on what in the model represents the interaction with the second axis (i.e., the state corresponding to link 3 velocity in this case) because that is the most uncertain part.

Figure 5.15 shows two details of the velocity reconstruction of link 2 with the 6-state Kalman filter with the above covariance matrices.

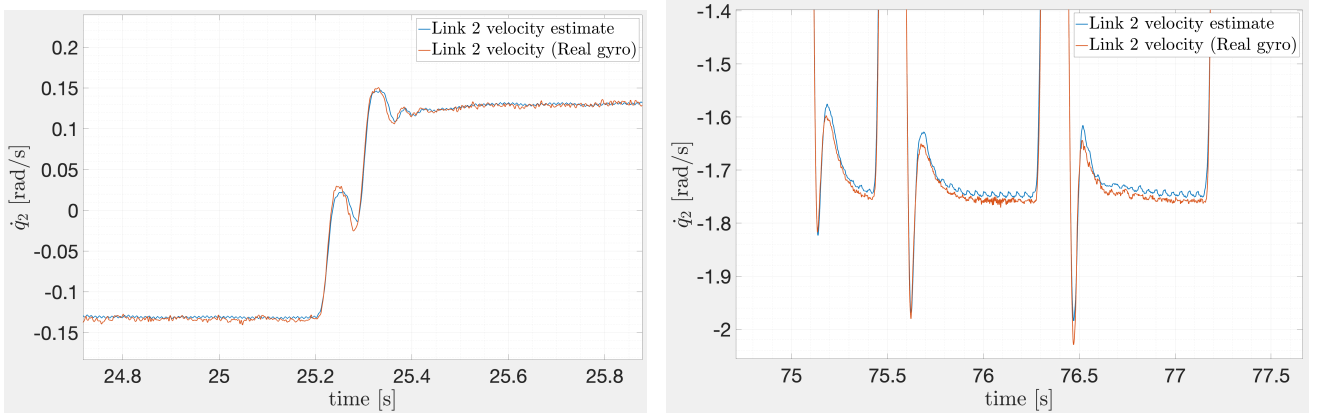


Figure 5.15. Link 2 velocity reconstruction using 6-state Kalman filter with identified data and real gyroscope (zoom)

We see that with higher gains there is a more plausible reconstruction of the state that takes less into account the model's oscillations.

5.6.2 Exciting trajectory

A more exciting program was made to see if the test signal had not high enough energy to let us see all the information. A data set is added to energize the vibration modes of the structure (a pseudo-random waveform generator was used to energize it more completely). The test signal contains frequencies between 10 and 25 Hz (this is the area in which, with this configuration of the link, on axis 2 we can see the vibrating phenomenon). The current has a dynamic range from 0 to 7 Ampères. These acquisitions are almost the equivalent of what we had in simulation.

Figure 5.16 shows the link 2 velocity reconstruction of the 6-state Luenberger observer with identified data superimposed to the real gyroscope with the exciting trajectory and a zoom into an area.

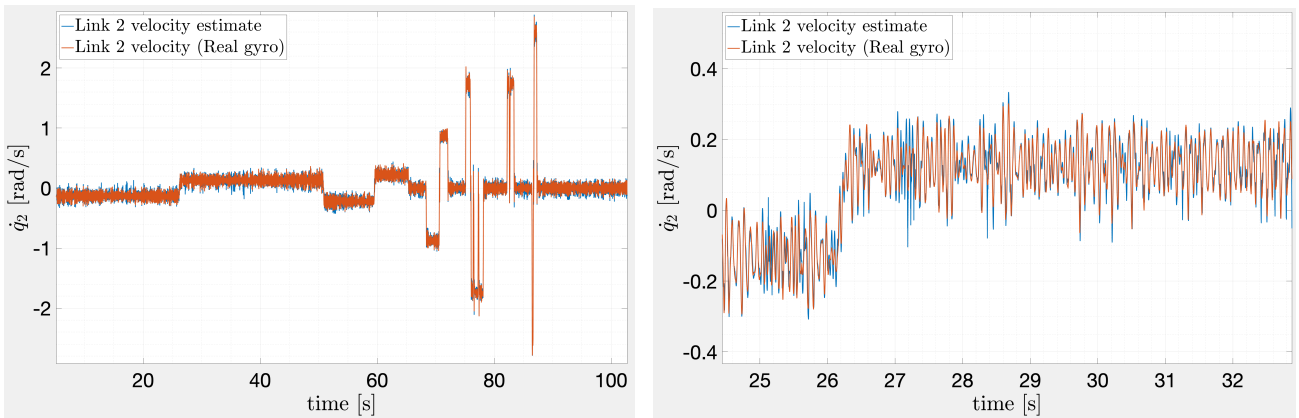


Figure 5.16. Link 2 velocity reconstruction of the 6-state Luenberger observer superimposed to real gyroscope (exciting trajectory) and relative zoom (right)

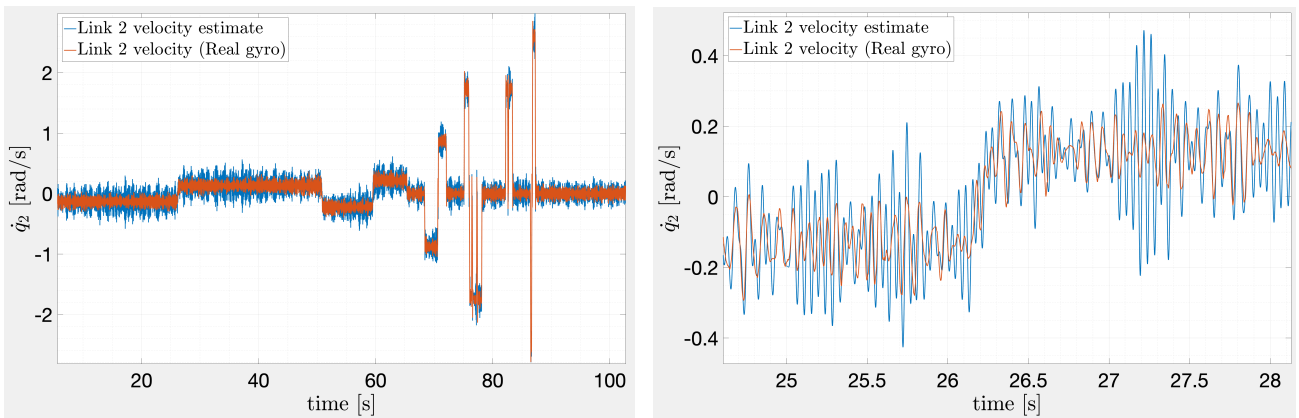


Figure 5.17. Link 2 velocity reconstruction of the 6-state Kalman filter superimposed to real gyroscope (exciting trajectory) and relative zoom (right)

Figure 5.17 shows the link 2 velocity reconstruction of the 6-state Kalman filter with identified data superimposed to the real gyroscope with the exciting trajectory and a zoom into an area.

As before, we see that the oscillations in the case of the 6-state Kalman filter are much more highlighted. By changing the covariance matrices as mentioned in the previous section, the result is shown in Figure 5.18.

As before, by increasing the correction action of the filter the reconstruction has much less oscillations and is much better.

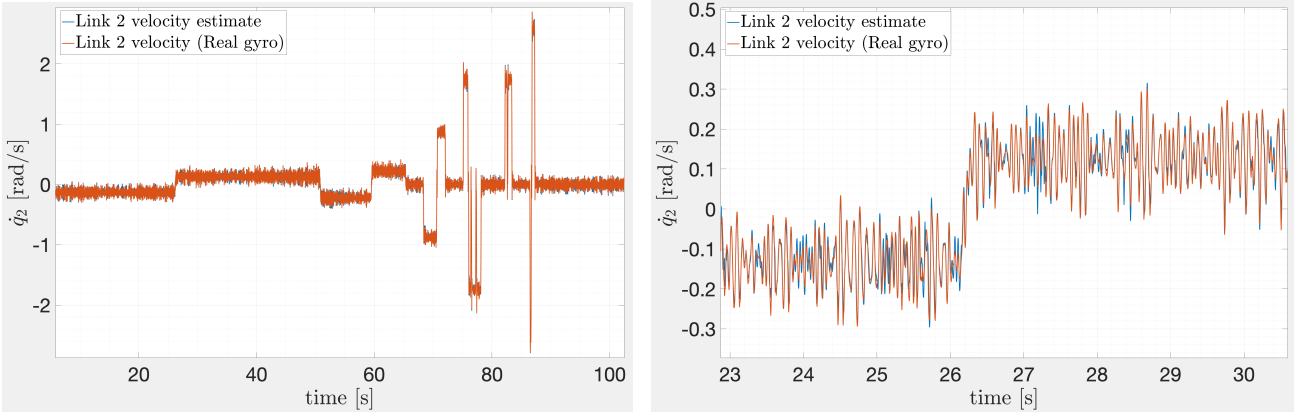


Figure 5.18. Link 2 velocity reconstruction of the 6-state Kalman filter superimposed to real gyroscope (exciting trajectory) and relative zoom (right)

5.6.3 Final results with real gyroscope

Tables 5.3 and 5.4 show the fit percentages obtained with all types of observers compared with the real gyroscope with the 400 Hz acquisition.

| N. states | Kalman filter | | |
|-----------|----------------------|----------------|-----------------|
| | Disturbance observer | Nominal data | Identified data |
| 6-state | YES | 95.0502 | 95.0812 |
| | | 97.9497 | 97.9565 |
| 5-state | NO | 97.5994 | 98.2280 |
| 7-state | NO | 97.9799 | 98.0004 |

Table 5.3. Kalman filter results on real data (Xsens gyroscope - 400 Hz)

| N. states | Luenberger observer | | |
|-----------|----------------------|----------------|-----------------|
| | Disturbance observer | Nominal data | Identified data |
| 6-state | YES | 97.9236 | 98.0433 |
| 5-state | NO | 97.6289 | 98.0528 |
| 4-state | YES | 97.8717 | 98.0949 |

Table 5.4. Luenberger observer results on real data (Xsens gyroscope - 400 Hz)

Tables 5.5 and 5.6 show the fit percentages obtained with all types of observers compared with the real gyroscope with the exciting trajectory.

As seen from the plots, also from the fit percentages we can see that the 6-state Kalman filter with a greater correction action (second row of the table) is much better than the other (first row).

The result of the 4-state Luenberger observer seems to suggest to maintain a minimal description of the dynamics of axis 2 for the observer model.

| N. states | Kalman filter | | |
|-----------|----------------------|----------------|-----------------|
| | Disturbance observer | Nominal data | Identified data |
| 6-state | YES | 62.5290 | 79.5595 |
| | | 90.8822 | 93.5114 |
| 5-state | NO | 89.3559 | 92.7743 |
| 7-state | NO | 90.8286 | 93.9836 |

Table 5.5. Kalman filter results on real data (Xsens gyroscope - exciting trajectory)

| N. states | Luenberger observer | | |
|-----------|----------------------|----------------|-----------------|
| | Disturbance observer | Nominal data | Identified data |
| 6-state | YES | 91.3721 | 93.4999 |
| 5-state | NO | 89.6073 | 93.2436 |
| 4-state | YES | 90.1289 | 93.8911 |

Table 5.6. Luenberger observer results on real data (Xsens gyroscope - exciting trajectory)

The best Kalman filter is the 7-state one that has a simpler model but interprets the interaction with the outside world through a resonant low pass filter.

The tests with the real gyroscope are the most significant, because they allow to understand that what seemed an apparent faulty reconstruction of the observers actually took into account the fact that there were no vibrations.

It is important to see that the results with identified data are always much more better than those with nominal data.

6. Conclusions

In this thesis, different kinds of observers have been designed to estimate the state (link velocity) of a two-link non-rigid industrial manipulator. In a particular simplified condition in which there is only one axis moving at a time, the objective was to understand how faithfully the dynamics of the machine can be reconstructed using simple single axis models, trying to reconstruct the action of non-linear frictions well and defining a minimum order model.

The compensation of Coulomb friction in feedforward or a second adjustment ring (Disturbance observer) are the resources that allow the observer to take into account the presence of friction acting on the motor axis. If there is a band separation, and the external part works on the low frequency and has a proportional-integral structure, it manages to reconstruct the friction very well, because friction is like a non-linear feedback of proportional-integral nature on a speed.

The added value of the thesis is to see if we can define the dynamics of axis 2 as its own dynamics as if it were an isolated axis plus an additional dynamics linked to some observable (non-measurable) state, so that the complexity of the model of the observer is reduced. Various models were tested:

- In the 6-state observer, the complete model that also contains the braked axis 3 is used to better describe the reality of the physical plant. The modal interaction part is entirely reconstructed by the observer, the friction part on the motor is estimated by the disturbance observer (separation of the effects). This representation is very demanding (in addition to the parameters of axis 2, the rest of the structure should be known well: it requires a very refined model).
- In the 5-state observer, a state is added to the nominal model to take into account all the unmodeled parts. The 5th state helps to reconstruct the frequency response, especially if the gains are high. Unfortunately, the observer also puts motor friction on the additional state. Therefore, I can no longer distinguish what is friction on the motor from what is transmitted torque.
- In the 4-state observer, no states are added to the nominal model of the isolated axis 2. The model does not include inertial couples.
- The 7-state observer is a more sophisticated system: the additional state is powered by its own dynamic block (a filter that is synchronized in the frequency range in which the interaction between axes 2 and 3 is expressed). This step is the added value compared to the state of the art.

For each model two different approaches are tested:

1. Luenberger observers, whose gain matrix have been evaluated through a pole placement technique.
2. Kalman Filter, whose gain matrix have been obtained tuning Q and R covariances.

In a simulation environment, we managed to reproduce a good reconstruction of the state (reducing a lot the gain) both with the Kalman filter and with the asymptotic Luenberger observer. However, it is an ideal and simplified scenario. In the considered context we had a lot of information (because with the white noise the plant was energized well) and the plant had simplified frictions. One of the limitations of simulation tests is that the plant is a linear model. In reality, the linear model approximates a dynamic that is not linear. Furthermore, a scenario was studied where all the friction is attributed to the motor and there is no friction on the load.

As far as real data are concerned, the virtual gyroscope collects information from the machine when the dynamics is fast, it is well energized and the non-linear friction that acts is unable to dampen the vibrations. The prediction made with a linear model deduced from the identification does not allow to see the damping action of friction, which instead it is shown by the real gyroscope. We can say that both in a normal signal context and with a more energized signal, all the tested observers work well. The interesting thing is that the Kalman filter for a model that has a nominal part and a part that tries to simulate the uncertainty, gives the best reconstruction. In conclusion, if it is possible to represent the uncertain part of reality (even in an approximate way), the observer tends to function better.

Model complexity and performance

There is a tradeoff between model complexity and performance: if the model is very close to reality (6-state observer) then the reconstruction of the state in simulation is excellent even with low gains (there is less need to correct the estimate); if instead a 4th order model is considered, even if a state that should take into account the unmodeled parts is added, a good reconstruction of the state of interest can be obtained only with very high gains (the correction action balances the missing parts of the model), but noise sensitivity problems increase. It is therefore important that, given the same noise model, if we want to reduce the sensitivity of the state estimate, we need to use a more complex model.

The conclusion that can be drawn from the obtained results with real data is that it is always better to have a strong correction action, because it allows to see those things that the predictive model does not take into account. We have indirect information on the state we need (the measures we take are upstream of the state we are interested in) so we need to increase the correction action.

Sensitivity to disturbances

Observers work well only if all cause and effect relationships are known and represented. The observer guarantees in closed loop that the tracking of the measured motor position is good, but it is sensitive to the presence of measurement disturbances and unmodeled torque disturbances, and therefore forces non-congruent trends on the reconstruction of the other state variables.

In particular, the simulations tell us that to have a very good reconstruction of the state variables, we must reconstruct the action of friction.

Identified and nominal data

Using a better identified model, the quality of the reconstruction is better than with a first approximation model, and therefore better results can be obtained. Deviating from a precise model, the reconstruction of the state is good for the measurement (motor position), but is not very significant for all the other states.

Final conclusion

In conclusion, for a good reconstruction of the state we must have:

- A good model very close to reality
- A way to compensate for the unknown part of the model (that part that is relevant to the functioning of the real system that we cannot explicitly represent in the model)
- A reasonable calibration of the observer gains, with a very strong correction action
- A model of all the disturbance signals that act on the system: all those that are not represented or compensated lead to reconstruction errors.

Future works

Some analyses could be done for future applications:

1. The presence of very high initial transient states should be avoided, tuning the initial conditions in a better way (now they are set to zero)
2. In this work the analysis was carried out of a movement program in which the inertia sub-matrix related to axes 2 and 3 does not vary when the position of the manipulator varies. The nature of the Linear Parameter Varying (LPV) system should be analyzed by updating the matrices every 10 ms. Otherwise, an adaptive re-evaluation based on the varying trend of the matrix could be applied.
3. A more complex friction model could be used.
4. Kalman filtering theory should be strengthened to understand how properly select covariance matrices.
5. Disturbance robustness to non-modeled parts should be revised and improved.
6. The final test done with the real gyroscope could be improved through a fine calibration between the three axes of the sensor and the rotation axis of the link. A careful calibration of the instrument would imply a separate procedure (in this case it was done visually).

Bibliography

- [1] G. F. R. Ellis, “Observers in control systems: A practical guide”, 2002.
- [2] A. De Luca and W. J. Book, “Robots with flexible elements”, in *Springer Handbook of Robotics*, B. Siciliano and O. Khatib, Eds. Cham: Springer International Publishing, 2016, pp. 243–282.
- [3] H. Ullah, F. M. Malik, A. Raza, I. Ahmad, N. Mazhar, and R. Khan, “Tracking control of flexible joint single link robotic manipulator via extended high-gain observer”, in *2021 International Bhurban Conference on Applied Sciences and Technologies (IBCAST)*, 2021, pp. 630–635.
- [4] M. Hamad, “Modelling and feed-forward control of robot arms with flexible joints and flexible links”, 2016.
- [5] V. Lertpiriyasuwat, M. C. Berg, and K. W. Buffinton, “Extended kalman filtering applied to a two-axis robotic arm with flexible links”, *The International Journal of Robotics Research*, vol. 19, pp. 254–270, 2000.
- [6] S. Akhlaghi, N. Zhou, and Z. Huang, “Adaptive adjustment of noise covariance in kalman filter for dynamic state estimation”, in *2017 IEEE Power Energy Society General Meeting*, 2017, pp. 1–5.
- [7] S. E. Talole, J. P. Kolhe, and S. B. Phadke, “Extended-state-observer-based control of flexible-joint system with experimental validation”, *IEEE Transactions on Industrial Electronics*, vol. 57, no. 4, pp. 1411–1419, 2010.
- [8] A. A. Godbole, J. P. Kolhe, and S. E. Talole, “Performance analysis of generalized extended state observer in tackling sinusoidal disturbances”, *IEEE Transactions on Control Systems Technology*, vol. 21, no. 6, pp. 2212–2223, 2013.
- [9] Y. Du, W. Cao, and J. She, “Analysis and design of active disturbance rejection control with an improved extended state observer for systems with measurement noise”, *IEEE Transactions on Industrial Electronics*, vol. 70, no. 1, pp. 855–865, 2023.
- [10] W. Wei, B. Liang, D. Li, and W. Su, “Improving the efficiency of extended state observer under noisy measurements by low-pass filter”, in *2016 Chinese Control and Decision Conference (CCDC)*, 2016, pp. 3566–3569.
- [11] H. Sun, R. Madonski, S. Li, Y. Zhang, and W. Xue, “Composite control design for systems with uncertainties and noise using combined extended state observer and kalman filter”, *IEEE Transactions on Industrial Electronics*, vol. 69, no. 4, pp. 4119–4128, 2022.
- [12] S. Panzieri and G. Ulivi, “Design and implementation of a state observer for a flexible robot”, in *[1993] Proceedings IEEE International Conference on Robotics and Automation*, 1993, 204–209 vol.3.

- [13] L. Le Tien, A. Albu-Schaffer, A. De Luca, and G. Hirzinger, “Friction observer and compensation for control of robots with joint torque measurement”, in *2008 IEEE/RSJ International Conference on Intelligent Robots and Systems*, 2008, pp. 3789–3795.
- [14] W.-H. Chen, D. Ballance, P. Gawthrop, and J. O’Reilly, “A nonlinear disturbance observer for robotic manipulators”, *IEEE Transactions on Industrial Electronics*, vol. 47, no. 4, pp. 932–938, 2000.
- [15] T. De Vries, E. Coelingh, E. Schrijver, and J. Dijk, “Design of disturbance observers for the compensation of low-frequency disturbances”, Jan. 2000.
- [16] M. W. Spong, “Modeling and control of elastic joint robots”, *Journal of Dynamic Systems Measurement and Control-transactions of The Asme*, vol. 109, pp. 310–319, 1987.
- [17] K. J. Aström and B. Wittenmark, *Computer Controlled Systems: Theory and Design*. Prentice Hall, 1984.
- [18] C. Canudas de Wit, H. Olsson, K. Astrom, and P. Lischinsky, “A new model for control of systems with friction”, *IEEE Transactions on Automatic Control*, vol. 40, no. 3, pp. 419–425, 1995.
- [19] P. R. Dahl, “A solid friction model”, 1968.
- [20] A. Bottero, G. Gerio, V. Perna, and A. Gagliano, “Adaptive control techniques and feed forward compensation of periodic disturbances in industrial manipulators”, Sep. 2014.
- [21] A. Bottero, *Hard material small-batch industrial machining robot hephestos final project review wp4: Robot advanced position control for machining*, Dec. 2015.